Integral Synthesis and Clearance Analysis via DIA (ISDia) Reveals Coordinated Protein Dynamics Regulation during Endoplasmic Reticulum Stress

Yue Dou[1], Danny Qiu[1], Vivien Li[1], Maja E. Wierzbińska[1], Gregory R. Keele[2], Wenpeng Liu[1], Jie Yang[1], Joao A. Paulo[3], Ling Qi[4], Tian Zhang[1,*]

[1] Department of Biochemistry and Molecular Genetics, School of Medicine, University of Virginia, Charlottesville, VA 22903, USA

[2] Research Triangle Institute International, Research Triangle Park, NC 27709, USA

[3] Department of Cell Biology, Harvard Medical School, Boston, MA 02115, USA

[4] Department of Molecular Physiology and Biological Physics, School of Medicine, University of Virginia, Charlottesville, VA 22903, USA

* Corresponding author. Email address: tian_zhang@virginia.edu

SUMMARY

ER stress disrupts protein homeostasis and impacts protein dynamics, driving cellular responses critical for survival, development and disease. However, no current proteome-wide technology enables simultaneous identification of proteins undergoing altered synthesis and clearance and distinguish their relative contribution during ER stress. To fill this gap, we developed Integral Synthesis and clearance analysis via DIA (ISDia), a robust mass spectrometry-based platform that integrates pulsed-SILAC labeling with data-independent acquisition (DIA) to quantify heavy and light peptide changes and determine the drivers of protein dynamics with high proteome coverage under non-steady-state conditions. Using ISDia, we uncover diverse regulatory mechanisms by which protein synthesis and clearance are modulated to control protein abundances during ER stress, revealing PERK dependent and independent regulatory mechanisms across subcellular compartments, complexes and isoforms. These findings highlight the potential of ISDia as a powerful and widely applicable platform for elucidating protein dynamic regulatory mechanisms.

INTRODUCTION

Proteins within cells are in a state of dynamic turnover[1]. This delicate balance is achieved by tight regulation of protein synthesis, protein folding and protein degradation, which maintains cellular homeostasis[2,3]. The endoplasmic reticulum (ER) is responsible for maturation of around 40% of the proteins in the eukaryotic cells[4]. Accumulation of misfolded or unfolded proteins within the ER lead to activation of the unfolded protein response (UPR). The primary function of UPR is to restore protein homeostasis by reducing protein synthesis, upregulating molecular chaperones, and promoting the degradation of misfolded proteins by ER-associated degradation (ERAD)[5–7]. Dysregulation of the UPR is implicated in various diseases, including metabolic syndromes, cancer, immunological disorders and neurodegenerative conditions[5,6]. Understanding how protein dynamics is modulated

in response to ER stress illuminates how cells respond to stress in diseases and why UPR failure can lead to disease progression[5]. Although nucleotide sequencing and proteomics technologies have revealed how transcriptional and protein turnover regulation contribute to protein homeostasis restoration in response to ER stressors[8,9], they fail to distinguish the respective roles of protein synthesis and degradation in regulating protein abundances. This gap has highlighted the need for quantitative approaches that deconvolute distinct regulatory layers governing protein dynamics.

Advances in mass spectrometry have enabled proteome-wide analysis of protein turnover, providing insights into the regulation of the proteome across diverse biological systems, including cell lines, mouse models and single cells[10–15]. Pulsed Stable Isotope Labeling by Amino Acids in Cell Culture (pSILAC) is a widely used metabolic labeling technique that enables the quantitation of protein turnover by incorporating isotopically labeled amino acids into proteins[16]. In pSILAC experiments, heavy peptide intensities represent newly synthesized peptides, whereas light peptide intensities represent pre-existing peptides. At the steady state in the protein synthesis and protein clearance (i.e., the sum of protein degradation and dilution effect of cell division) rates are equal, the protein turnover rate can be calculated by fitting H/L ratios at different time points based on first-order kinetics[17]; tracking of heavy peptide and light intensity, as well as cell division will enable separating absolute protein synthesis and degradation with the effect of cell division in protein dynamics[18]. However, under many biological processes, including stress responses, drug treatments, and cell differentiation, cells often deviate from steady-state conditions and the assumptions underlying the kinetic model are not met; in addition, cells may undergo cell cycle arrest or cell death, making cell division rate tracking impossible. Instead, direct comparison of heavy and light peptide intensities across different conditions enables comparison of the relative contributions of protein synthesis and clearance and identification of the drivers of protein dynamics without calculating exact rates under steady state conditions.

In data dependent acquisition (DDA) workflows, the H/L ratios are often used instead of raw intensities for protein turnover analysis, as DDA workflows restrict accurate protein quantitation due to sampling inconsistency in abundance-based MS2 selection across samples, especially with the co-existence of the heavy and light peptides. This inconsistency prevents reliable cross-sample intensity comparisons for pre-existing and newly synthesized peptides, making it challenging to determine the contribution of protein synthesis and clearance to protein dynamics under non-steady state conditions. Integrating pSILAC with tandem mass tags (TMT) enables the relative measurement of pre-existing proteins and newly synthesized proteins across samples, allowing for multiplexed analysis of protein synthesis and degradation, respectively[18,19]. However, in addition to the inherent limitations of TMT experiments, such as a restricted number of tags, ratio compression, and the requirement for extensive fractionation, it remains challenging to obtain high-quality MS2 spectra for both heavy and light peptides for accurate quantitation of protein abundance and turnover dynamics without extensive fractionation and complicated data analysis[14,18,20]. These limitations limits TMT studies for accurately measuring protein dynamics in complex scenarios.

Recent advances in data-independent acquisition (DIA) mass spectrometry have enabled deeper proteomic analysis[15,21]. Unlike DDA, which preferentially detects abundant proteins and often misses low-

abundance species[22], DIA fragments all peptides within a defined mass-to-charge (m/z) range, providing comprehensive and unbiased proteome coverage[23]. Previously, pSILAC has been coupled to DIA to measure protein degradation[14,15,24,25]. The Asymmetric Track Lossless (Astral) analyzer of the Orbitrap Astral mass spectrometer enables acquisition of high-resolution, accurate-mass (HRAM) MS/MS spectra at rates of up to 200 Hz. Parallel acquisition using the Orbitrap and Astral analyzers allows for full scans with high dynamic range and resolution, as well as fast and sensitive HRAM MS/MS scans, further expanding proteome coverage and ensuring quantitative accuracy[26–30]. The Orbitrap Astral mass spectrometer has been shown to enhance DIA quantitation through its increased speed, sensitivity, and dynamic range, enabling consistent detection and quantification across multiple sample[21,31].

In this study, we leverage recent advances in high-sensitivity MS instrumentation and DIA strategies to develop ISDia (Integral Synthesis and Clearance analysis via DIA), a streamlined platform with simplified sample preparation and data analysis workflows that enables proteome-wide identification of proteins with altered synthesis and clearance and distinguishing their relative contributions to protein dynamics. We first established the feasibility of this approach by quantifying the intensities of heavy isotope-labeled peptides (heavy), non-heavy isotope-labeled peptides (light), their sum(H+L), as well as calculating the H/L ratio of pre-defined standards with various H/L ratios. We established ISDia by combining multiple time points from pSILAC labeling experiments into a single sample, enabling direct comparison of peptide intensities across conditions. This approach eliminates the need for synthesis and degradation rate calculations, thereby extending its applicability to non-steady-state conditions[32]. By integrating changes in heavy intensity, light intensity, H+L and H/L ratios, ISDia quantifies protein dynamics and delineates the contributors underlying protein dynamics changes.

We then applied ISDia to investigate protein dynamics during ER stress, revealing that cells displayed coordinated synthesis and clearance through diverse regulatory mechanisms to control protein abundance across individual proteins, subcellular compartments and protein complexes. We applied ISDia to PERK$^{-/-}$ cells and systematically explored the PERK-dependent and independent regulation during the UPR. We found that mitochondrial protein synthesis is selectively preserved during the global suppression in a PERK-dependent manner, while proteins in the ER are differentially regulated in a PERK-independent manner. Moreover, protein complex analysis revealed PERK-mediated isoform-specific regulation of p97/VCP during the UPR. Altogether, our study presents a robust and versatile proteomics platform for quantifying the relative contributions of protein synthesis and clearance to proteome remodeling under non-steady-state conditions with high proteome coverage, while uncovering mechanistic insights into the regulation of protein homeostasis during ER stress.

RESULTS

DIA expands the coverage of pSILAC experiments and reduces variation among replicates To establish ISDia, we first assessed whether heavy and light intensities instead of H/L ratios, can be used for protein dynamics analysis in pSILAC experiments. We generated MS standards with predefined H/L ratio by mixing light-labeled cells and fully heavy-labeled cells at H/L ratios of 1:1, 3:1, 9:1, and 27:1 (**Fig. 1A**). Standards were prepared in triplicate and analyzed on an Orbitrap Astral mass spectrometer employing both DDA and DIA methods with 50

min. gradients. Equal amounts of peptides were injected across all runs. DDA raw files were processed with FragPipe, while DIA files were analyzed using Spectronaut in directDIA mode. For quantitation, MS1-level data were used for DDA, and MS2-level data were used for DIA to quantify heavy and light peptides (**Fig. 1A**).

To optimize Spectronaut settings for analyzing pSILAC-DIA data acquired on the Orbitrap Astral mass spectrometer, we systematically evaluated three different parameters: *in silico* generation of missing channels, spike-in channels and cross-run normalization (**Fig. S1A**). Although the *in silico* generation of missing channels increased the total number of quantified proteins (**Fig. S1B**), it resulted in fewer proteins with coefficient of variation (CV) less than 20% (**Fig. S1C**), suggesting reduced quantitation accuracy. Additionally, neither *in silico* generation of missing channels nor the use of spike-in channels improved proteome coverage or quantitation accuracy (**Fig. S1D**). In contrast, cross-run normalization improved quantitation accuracy when the H/L ratio was high (**Fig. S1B-D**). Based on these results, we used only cross-run normalization for all subsequent analysis in this study.

We then compared the performance of DIA and DDA approaches in protein quantitation. Notably, the DIA method enabled the quantitation of both heavy and light intensities for over 10,000 proteins at each mixing ratio in a single run, whereas DDA quantified fewer proteins (**Fig. 1B**). Using DIA, the number of quantified proteins ranged from 9552 to 9963 across three replicates at each mixing ratio, respectively. To assess the reproducibility using the Orbitrap Astral DIA workflow, we calculated the CV across three replicates for light peptide intensity, heavy peptide intensity, total intensity, and H/L ratio at each mixing ratio. A CV threshold of 20% was applied to filter out proteins with high variability. Using DIA, 7895, 7285, 6245, and 4930 proteins met the 20% CV threshold across all four metrics (heavy intensity, light intensity, H+L, and H/L ratio) for the respective mixing ratios. In contrast, DDA yielded 1763, 1868, 911, and 671 proteins that passed the same criteria (**Fig. 1B**). DIA consistently showed significantly lower CVs compared to DDA, indicating that DIA provided more consistent protein quantification across replicates (**Fig. 1C-F**). We observed that the CVs for the intensities of light peptide (**Fig. 1C**) were higher than those for heavy peptides (**Fig. 1D**) and for total intensities (**Fig. 1E**) across both acquisition methods. As the light intensity decreased in standards with more extreme H/L ratios, the CVs for both light intensities and H/L ratios increased (**Fig. 1C, Fig. 1F**), highlighting the challenges associated with accurately quantifying low intensity precursors.

To further investigate the relationship between proteome coverage and peptide intensity, we compared DIA intensities between proteins quantified by both methods and those quantified exclusively by DIA. The majority of proteins quantified by DDA were also quantified with DIA (>75%) (**Fig. 1G**). Proteins quantified exclusively by DIA exhibited lower light (**Fig. 1H**) and heavy (**Fig. S2A**) intensities than those quantified by both methods. Proteins quantified exclusively by DDA exhibited no difference for either light (**Fig. S2B**) or heavy (**Fig. S2C**) precursor intensities with the overlapping proteins. These results indicated that pSILAC-DIA on the Orbitrap Astral mass spectrometer can mitigate the challenge of low intensity precursors and improve proteome coverage and reproducibility across replicates.

DIA enhanced quantification accuracy within and across samples We further investigated whether DIA accurately quantifies heavy and light intensities within individual samples. The DIA method showed higher accuracy and lower standard deviations (s.d.) within samples compared to the DDA method at the expected H/L ratios before and after applying the 20% CV cutoff for both light (**Fig. 2A-D**) and heavy peptide intensity (**Fig. S3A-B**). Standard deviations increased with higher H/L mixing ratios, again highlighting the challenge of accurately measuring H/L ratios in pSILAC experiments with extreme labeling conditions. Moreover, to evaluate whether DIA enabled accurate quantitation across samples, we normalized heavy and light intensities across different samples using the H/L ratio 1:1 sample as a reference. The result indicated that the DDA measurements deviated and failed to provide accurate results (**Fig. 2E**). In contrast, DIA measurements recapitulated the heavy and light peptide intensity differences across samples with cross-sample normalization setting in Spectronaut searches[14,33] (**Fig. 2F, Fig. S3C**). Overall, these results indicated that light and heavy peptide intensities can be directly used for cross-sample comparison in DIA, highlighting their potential for analyzing protein synthesis and clearance.

Systematic evaluation of High-Field Asymmetric Waveform Ion Mobility Spectrometry (FAIMS) and acquisition parameters for pSILAC-DIA FAIMS separates ions based on their differential mobility in high and low electric fields, allowing for better resolution of overlapping or co-eluting peptides with reduced background noise and interference[34,35]. To test whether incorporating FAIMS will increase the number of quantified proteins and improve quantitation accuracy in pSILAC-DIA experiments, we first tested a range of single compensation FAIMS voltages for DIA method and identified -50V as the compensation voltage which quantified the highest number of proteins (**Fig. S4A**). We next analyzed standards with pre-defined H/L ratios of 1:1 and 9:1 with the in-line FAIMS source connected and evaluated its impact on quantitation of light peptides, heavy peptides, their combined intensities and the H/L ratio. FAIMS did not yield any significant improvement in protein coverage or quantitation accuracy (**Fig. S4B-C**). Using a 2 m/z isolation window quantifies more proteins than a 4 m/z isolation window (**Fig. S4B)**. Different injection times within each setting had minimal effects on protein coverage (**Fig. S4B**) and on CVs of the heavy, light and total intensities (**Fig. S4C**). Thus, a 2 m/z isolation window and an injection time of 3.5 ms for DIA scan without FAIMS were used for following DIA data acquisition.

Development of the ISDia method to investigate protein synthesis and clearance dynamics regulation during ER stress We confirmed the activation of key factors of the UPR and their effects on downstream targets by the N-glycosylation inhibitor tunicamycin (Tm) and the SERCA inhibitor thapsigargin (Th). Treatment of HeLa cells under both these conditions rapidly induced IRE*α*-mediated splicing of X-box Binding Protein 1 (XBP1) mRNA and production of XBP1s protein, detectable by Western blot after 2h (**Fig. S5A**). In a proof-of-principle experiment, cells were treated with DMSO, Tm, or Th at the initiation of isotope labeling. Samples were harvested at 6, 12, 24 and 48h post-treatment in biological triplicates. Inspired by proteome integral stability alternation (PISA) which combines samples originating from different temperatures of the same perturbation to reduce the number of samples analyzed[36,37], we pooled equal amounts of protein from samples collected at each time point following treatments for MS analysis and proposed a simplified approach that

infers changes in protein synthesis, clearance and protein abundance by directly comparing integrated light, heavy intensities and H+L across conditions. We term this method Integral Synthesis and clearance analysis via DIA (ISDia) (**Fig. 3A**). We quantified light, heavy peptide intensities and calculated their sums and ratios for approximately 9,000 proteins across all three conditions (**Fig. 3B, Table S1**). Notably, each metric reflected the dynamic changes occurring throughout the treatment period, rather than representing a single endpoint measurement. This streamlined design enabled protein dynamics analysis under non-steady state conditions and reduced the number of required samples from twelve to three per condition, significantly decreasing both instrument and data processing time. By combining peptides, ISDia also minimizes quantitation biases arising from peptides with extreme H/L ratios and insufficient signal in either channel (**Fig. 1C**), thereby improving quantitative accuracy and expanding proteome coverage. Additionally, this sample design enables statistical analysis under various conditions.

HSPA5, also known as ER chaperon BiP, operates as a Hsp70 chaperon in complex with its cochaperone proteins and as a sensor of ER stress and activates UPR, with its expression upregulated under UPR[9,38,39]. In our dataset, HSPA5 exhibited an increased heavy and light intensity (**Fig. 3C**) with higher H/L ratio (**Fig. 3D**) under both Tm and Th treatment, indicating that enhanced protein synthesis is the primary driver of its increased abundance in the process. Global analysis revealed that, under ER stress induced by Th and Tm treatments, proteins showed increased light intensities, decreased heavy intensities and H/L ratios, while the sum of heavy and light intensities remained relatively stable compared to DMSO controls (**Fig. 3E-F**). These patterns suggest a global reduction in both protein synthesis and clearance, potentially driven by slower cell division rates and additional protein dynamics regulatory mechanisms. Changes in heavy, light peptide intensities and their sum, as well as H/L ratios, following Th and Tm treatments were highly correlated in the ISDia dataset (**Fig. S5B-E**). In summary, these results demonstrate that ISDia captures changes in heavy and light peptide intensity, uncovering the regulatory mechanisms underlying protein dynamics.

We next compared the ISDia method with a single-timepoint pSILAC-DIA approach, which requires equivalent instrument time. Using samples labeled for 48 hours, we quantified approximately 8,000 proteins across three replicates for light, heavy and total intensities (**Fig. S6A**), only showing a ~10% decrease in coverage compared to the ISDia method. We confirmed that the results from the 48-hour time point and the ISDia experiments were highly correlated (**Fig. S6B**). However, in the single time point experiment, applying a CV threshold of < 20% substantially reduced the number of proteins quantified with heavy, light intensity, H+L and H/L ratios under DMSO, Tm, and Th conditions, respectively (**Fig. S6C).** In comparison, ISDia quantified approximately 8,000 proteins under the same conditions when using a CV cutoff, demonstrating enhanced proteome coverage with more robust measurements (**Fig. S6D**), despite the changes between treated samples and DMSO control being slightly reduced (**Fig. 3E-F, Fig. S6E**).

Dynamic coordination of protein synthesis and clearance modulated proteome changes during ER stress To further investigate the regulatory mechanisms of protein dynamics during ER stress, we compared H+L changes against H/L ratio changes in Th treated cells relative to the DMSO control, revealing a significant

moderate correlation ($R = 0.34$, $p < 2.2e^{-16}$) (**Fig. 4A**). Changes in heavy and light peptide intensities were more strongly correlated ($R = 0.5$, $p < 2.2e^{-16}$) (**Fig. 4B**). To systematically dissect the contribution of protein synthesis and clearance to protein dynamics, we color-coded individual proteins based on corresponding heavy and light intensity changes under treatment conditions and grouped them accordingly (**Fig. 4A-B**). We observed that proteins with increased H+L and heavy, but not light peptide intensities (blue), were primarily regulated by protein synthesis, whereas those with increased H+L and light, but not heavy peptide intensities (green), were primarily regulated by protein clearance. Similarly, we found that proteins with decreased H+L and heavy but unchanged light peptide intensities (purple), were likely regulated by reduced synthesis (**Fig. 4A-B**).

Notably, proteins with increased heavy, light peptide intensities and increased H+L (dark pink) diverged into two distinct groups based on their H/L ratio changes, suggesting that synthesis and clearance may contribute differentially to their overall abundance changes. We performed enrichment analysis with gene ontologies (GO) on the subset of proteins with higher H/L ratio and found that these proteins were enriched for amino acid metabolic and amino acid biosynthetic processes (**Fig. 4C**), which are transcriptionally regulated by ATF4[40,41]. The proteins with lower H/L ratio were predominantly enriched for functions related to the electron transport chain in mitochondria and catabolic process (**Fig. 4D**). These results suggest that an increased H/L ratio may reflect elevated protein synthesis contributing to total protein abundance, whereas proteins with decreased H/L ratios likely do not exhibit increased synthesis under these conditions. Similarly, proteins with decreased heavy and light peptide intensities and abundance (yellow), the decline is primarily driven by enhanced protein clearance, with or without a concurrent reduction in protein synthesis. Enrichment analysis found that these proteins with decreased level under ER stress conditions relative to DMSO control (purple + yellow) were enriched in cell cycle-related categories, including chromosome segregation, nuclear division, and mitotic spindle assembly checkpoint signaling (**Fig. 4E**). ISDia revealed that protein synthesis and clearance can act independently or synergistically to modulate protein abundances, and different protein categories may rely on distinct regulatory mechanisms, with either synthesis or clearance serving as the drivers of protein abundances.

Interestingly, we observed a substantial number of proteins exhibiting both significantly decreased heavy and increased light peptide intensity as well as unaltered H+L (orange) during ER stress, suggesting coordinated downregulation of both synthesis and clearance (**Fig. 4A**). To examine whether the decreased protein synthesis is driven by the systematic translation inhibition and the cell cycle arrest mediated by PERK[42,43] involved in UPR, we applied ISDia to PERK$^{-/-}$ cells (**Table S2**) and analyzed how protein synthesis and clearance were modulated in response to ER stress. The knockout of PERK was validated by the absence of PERK protein expression in Western blotting analysis (**Fig. 4F**). In contrast to WT cells, ATF4 levels did not increase in PERK$^{-/-}$ cells during the UPR, indicating disruption of the PERK-eIF2α-ATF4 axis. However, XBP1 and BiP, downstream targets of the other two ER stress senor in the UPR, IRE1α and ATF6, respectively, were still upregulated under UPR conditions (**Fig. 4G**), confirming activation of the remaining arms of the UPR. ISDia quantified light, heavy peptide intensities, protein abundance and H/L ratios, for over 9,000 proteins

across each treatment condition in PERK$^{-/-}$ cells (**Fig. S7A**). Compared to WT cells, Tm and Th treated PERK$^{-/-}$ cells showed fewer changes in heavy, light peptide intensities and H/L ratios (**Fig. S7B**). Changes under Th and Tm treatment were highly correlated (**Fig. S7C**). Specifically, the proteins that have decreased clearance and synthesis under Th treatment in WT cells had less changes in PERK$^{-/-}$ cells (**Fig. 4H-I**, **Fig. S7D**), indicating that the suppression of protein synthesis and clearance were PERK-mediated. We performed GO enrichment and found that proteins not exhibiting significantly downregulated synthesis in PERK$^{-/-}$ cells were enriched in RNA splicing, localization and transport (**Fig. S7E**).

Differential regulation of protein synthesis and clearance across cellular compartments during the UPR

Organelles such as the ER and mitochondria and large protein complexes, are often equipped with distinct quality control and proteolytic mechanisms that maintain their abundances and functions[44–48], leading us to investigate the regulatory mechanisms of protein dynamics within these cellular compartments (CC). We found that different CCs have diverse changes on H+L, H/L ratios, light and heavy peptide intensities under Th treatment in WT cells (**Fig. 5A**). Among all the CCs, chromatin proteins had the greatest degree of decreased heavy intensity. Mitochondrial proteins showed relatively less decreased heavy intensities compared to other CCs in WT cells, suggesting that the protein synthesis was less inhibited compared to other CCs. In PERK$^{-/-}$ cells, we observed reduced variation among CCs compared to WT cells (**Fig. 5B**). We then compared changes in light peptide intensities, H+L and H/L ratios under Th treatment relative to DMSO between WT and PERK$^{-/-}$ cells (**Fig. S8A**). While H+L in selective compartments showed significant changes, all the compartments showed a significantly attenuated decrease in light peptide intensities in PERK$^{-/-}$ cells. Interestingly, changes in heavy peptide intensities in mitochondrial proteins were significantly altered in PERK$^{-/-}$ cells (**Fig. 5C)**, indicating that the regulation of mitochondrial protein synthesis during the UPR is PERK-dependent.

A recent study has shown that PERK-ATAD3A interaction created a localized environment that allows translation of nuclear-encoded mitochondria proteins[49,50]. To assess whether that is the regulatory mechanism, we compared the protein level of ATAD3A in WT and PERK$^{-/-}$ cells. ATAD3A levels increased in WT cells but not in PERK$^{-/-}$ cells during the UPR (**Fig. 5D**), implicating its involvement in protecting mitochondrial protein synthesis in UPR. We observed distinct patterns in protein dynamics for mitochondrial proteins in WT (**Fig. 5E**) and PERK$^{-/-}$ (**Fig. 5F**) cells. In PERK$^{-/-}$ cells, changes in heavy protein intensity, both upregulation and downregulation, were attenuated compared to WT cells (**Fig. 5F, Fig. S8B-C**). Proteins with increased abundance in WT cells were enriched in pathways related to organic acid and metabolism and catabolism (**Fig. 5G**), which is mainly driven by PERK-ATF4 axis. Proteins with decreased abundance were associated with mitochondrial organization and mitochondrial DNA replication (**Fig. 5H**), suggesting elevated mitochondrial stress and impaired mitochondrial dynamics, including fission[49,51–53]. In addition, we identified proteins exhibiting at least a 1.5-fold decrease in heavy intensity and decreased H+L in PERK$^{-/-}$ cells but not in WT cells. Notably, proteins with reduced H+L were significantly enriched in mitochondrial matrix protein import, including TIMM23, ROMO1, and TIMM17A (**Fig. 5I-J**). These changes indicate that PERK is also required for maintaining mitochondrial protein import machinery during the UPR.

We next focused on ER proteins, because the regulation of protein synthesis and clearance within the ER during the UPR is critical for restoring proteostasis. The results indicated that protein synthesis and clearance were coordinately regulated to alternate the expression of certain ER proteins (**Fig. S9A**). GO enrichment revealed that proteins with potential increased synthesis and abundance in WT cells under Th treatment were enriched in GOs related to response to ER stress, endoplasmic reticulum-associated degradation (ERAD), and ER protein transport (**Fig. S9B, Fig. S9C**). Proteins with decreased protein abundance and synthesis were enriched in sterol metabolic process and phospholipid biosynthetic process (**Fig. S9D, Fig. S9E).**

Dynamic control of synthesis and clearance across protein complex subunits during the UPR Proteins often function as components of dynamic protein complexes that are co-regulated in response to environmental or intracellular changes. The composition and abundances of these complexes can impact their overall complex functions, and the state of a cell can be affected by the abundance or activity of protein complexes[21,54]. While previous studies have demonstrated that interacting proteins involved in protein complexes can be co-regulated[10,14,55], how they are modulated through protein synthesis and clearance remains largely unexplored. To address this question, we used the protein complexes annotated in Ori *et al*[56] to determine whether protein complex regulation could be systematically attributed to changes in synthesis and clearance (**Table S3**). The majority of protein complexes exhibited decreased synthesis and clearance under UPR-inducing conditions in WT cells. However, a subset of complexes, including the presequence translocase-associated motor (PAM) complex, p97/VCP-VIMP-DERL1-DERL2-HRD1-SEL1L complex and ubiquitin ligase ERAD-L complex, displayed a synergistic increase in heavy and light peptide intensity under Th treatment (**Fig. 6A**).

The PAM complex is a mitochondrion complex essential for importing preproteins into the mitochondrial matrix[57–59]. The Th-induced increase in heavy and light intensities observed in WT cells was reduced in PERK$^{-/-}$ cells, indicating that this mitochondrial regulation is PERK-dependent (**Fig. 6B, Fig. S10A**). In contrast, the upregulation of heavy and light intensities for both the p97/VCP-VIMP-DERL1-DERL2-HRD1-SEL1L complex and the ubiquitin ligase ERAD-L complex were also observed in PERK$^{-/-}$ cells (**Fig. 6B, Fig. S10A**), suggesting PERK-independent regulation. These two complexes play key roles in ERAD[7,60,61], which can be further activated by the ATF6 and/or IRE1α-XBP1 during the UPR[6,62–65]. Interestingly, we also observed significant downregulation in the synthesis of spliceosome components, implying global alterations in RNA splicing in addition to XBP1-mediated transcriptional activation during ER stress (**Fig. 6B**). Despite these effects on the sum of heavy and light intensities, changes in H/L ratios were minimal (**Fig. S10B**).

To determine whether all subunits within a complex are regulated uniformly, we analyzed the regulation of individual components of the p97/VCP-VIMP-DERL1-DERL2-HRD1-SEL1L complex in WT cells (**Fig. 6C**). The RING finger E3 ubiquitin ligase SYVN1 (HRD1) and its cofactor SEL1L, a scaffold protein that stabilizes HRD1 and facilitates substrate recognition[61], both showed increased protein abundances, potentially driven by both enhanced synthesis. DERL1 and DERL2, which form the retrotranslocation channel for ERAD

substrates[66,67], remained largely unchanged. SELENOS (VIMP), which recruits p97/VCP to the ER membrane and coordinates its interaction with other ERAD components, showed a significant abundance increase. Strikingly, we found that the two isoforms of p97/VCP, a transitional ER ATPase that supplies energy for protein extraction during ERAD, were differentially regulated during the UPR (**Fig. 6C**).

Using isoform-specific peptide quantification (**Fig. 6D**), we found that peptides from the full-length isoform showed no significant changes in heavy and light intensity (**Fig. 6E**), whereas those from the shorter isoform exhibited significantly increased heavy and light intensity in WT cells (**Fig. 6F**). While the regulation of other subunits within the complex was conserved in PERK$^{-/-}$ cells, the upregulation of the short VCP isoform was absent at both the protein level and peptide levels (**Fig. 6G, Fig. S10C**), indicating that its regulation is PERK-dependent.

To investigate potential structural differences between the two isoforms of p97/VCP, we used AlphaFold3[68] to generate a hexameric structural model of the short isoform (UniProt ID: A0AP0T8A3) (**Fig. 6H, Fig. S10D**). The predicted structural model revealed an overall organization highly similar to the previously reported cryo-EM structures of the long isoform[69,70], consistent with conserved architecture in the AAA+ ATPase core domains. To examine isoform-specific features, we performed a structural alignment of their N-terminal regions (residues 1-200 in the long isoform and 1-155 in the short isoform). The alignment revealed that the long isoform contains an additional N-terminal segment (residues 1-45, shown in blue in **Fig. 6I**) that includes the first β-strand. This β-strand participates in an extended β-sheet packing, suggesting a potential role in stabilizing the N-terminal domain conformation of the long isoform (**Fig. 6I**). Given that the N-terminal region of p97/VCP is implicated in the binding of ubiquitin ligases and DUBs or other cofactors[71,72] and involved in diseases conditions[73], these structural differences raise the possibility that the two isoforms may exhibit differential binding specificity or regulatory interactions under various cellular stress conditions. Further biochemical and functional studies will be needed to determine whether the distinct N-terminal features contribute to isoform-specific roles in cellular proteostasis during the UPR.

In summary, our results provided preliminary support that protein complexes were regulated through coordinated synthesis and clearance, and that individual subunits within a complex can exhibit differential regulatory patterns. Using the ISDia method, we also uncovered PERK-dependent, isoform-specific regulation of VCP in modulating ERAD pathway during the UPR, providing new hypotheses for further mechanistic investigation.

DISCUSSION

Here, we developed and established ISDia as a streamlined platform that enables comprehensive measurement of protein dynamics and determines the relative contribution of synthesis and clearance within a single experiment. In contrast to traditional turnover rate calculations, which rely on steady-state assumptions, ISDia integrate information and determine the relative changes of protein synthesis and clearance without rates calculation, making it particularly well-suited to capture proteome remodeling under non-steady-state conditions such as ER stress. ER stress induced by Th or Tm triggers apoptosis[5,42,43], making tracking cell

division rate and delineating the contributions of synthesis and degradation from cell division difficult. By integrating changes in light and heavy peptides, their sums and H/L ratios, ISDia offers a comprehensive view of protein dynamics during ER stress. ISDia broadens the reach of protein dynamics analysis, enabling systematic investigation of proteome remodeling across diverse biological processes such as drug discovery, stress responses, and cell differentiation.

In pSILAC-based experiment, light peptide intensities reflect protein clearance due to degradation and dilution by cell division, whereas heavy peptide intensities represent the accumulative effects of both protein synthesis and clearance. As a result, the observed proteome-wide correlation between light and heavy peptide intensities is expected. However, this interdependence poses a major challenge for disentangling the relative contributions of synthesis and clearance, particularly when they are regulated synergistically. Moreover, in response to ER stress, newly synthesized proteins (heavy) can be misfolded proteins that have different clearance dynamics compared to the pre-existing proteins (light), making accurate estimation of synthesis and clearance rates, or their relative changes infeasible. Therefore, while ISDia provides a general hypothesis on whether protein synthesis is altered for certain proteins (e.g., dark pink, yellow in **Fig. 4A-B**), additional evidence is required. Notably, in non-dividing cell models, light peptide intensities in ISDia are only influenced by protein degradation and can therefore be used for protein degradation comparison across conditions.

Multiplexed proteome dynamics profiling (mPDP)[19] enabled the investigation of the causes and consequences of protein degradation in biological systems. Compared to it, ISDia produces higher proteome coverage and a simplified workflow by employing DIA. The reduced sample requirement in ISDia enables its integration into high-throughput workflows[74,75]. These features collectively highlight ISDia as a broadly applicable and scalable platform for proteome dynamics analysis.

Advances in high-sensitivity mass spectrometry were instrumental in achieving high proteome coverage and quantitation accuracy both within and across samples. To optimize data acquisition for isotope-labeled samples in DIA on the Orbitrap Astral mass spectrometer, we systematically evaluated different injection times, isolation windows, and the use of FAIMS and found optimal parameters. FAIMS did not improve protein coverage and quantitation accuracy, likely due to the exclusion of specific peptides resulting from the use of only a single compensation voltage[34]. The capacity of other mass spectrometers to enable accurate quantification in isotope-labeled DIA experiments remined to be systematically assessed.

Using ISDia, we uncovered coordinated regulation between protein synthesis and clearance during ER stress. When cells require increased protein abundances to adapt to stressors, the most time-efficient response involves simultaneous upregulation of synthesis and suppression of clearance. Modulation of either process alone is still a prevalent mechanism. As expected, proteins exhibiting increased synthesis and increased clearance are rare under stress conditions. These findings provide systematic evidence for the tight coupling between synthetic and clearance pathways in regulating proteome remodeling under stress. We further demonstrated that proteins exhibiting reduced synthesis and clearance showed attenuated changes in PERK$^{-/-}$ cells, suggesting that this regulation is PERK-dependent. This is consistent with the established role of PERK in driving global translational suppression and cell cycle arrest in response to ER stress[42,43].

In addition, our analysis of cellular compartments and protein complexes demonstrated that PERK plays a central role in mitochondrial protein regulation during the UPR, with minimal involvement in ER protein modulation. While ER proteostasis is mainly regulated by IRE1α and ATF6 during the UPR[6,62–65], our results support a model whereby mitochondria protein synthesis was protected from the PERK-mediated synthesis suppression during ER stress. The PAM complex was upregulated in WT cells but not in PERK$^{-/-}$ cells, while the TIM23 complex, including TIMM23, ROMO1 and TIMM17A[76,77], was markedly reduced in PERK$^{-/-}$ cells but maintained in WT cells. These findings suggest PERK maintained mitochondrial protein import during ER stress. Furthermore, we identified isoform-specific regulation of VCP mediated by PERK in response to UPR activation, providing a compelling example of how cells modulate protein abundances under stress. ISDia offers a powerful platform to investigate such isoform-specific regulation with high proteome coverage. These regulatory mechanisms provide an unprecedented, system level view of global protein homeostasis control highlighting the diverse strategies that cells employ to adapt to stress conditions.

We note that pooling samples across time points effectively captures the averaged responses and highlights overarching trends. However, this approach is likely to be less sensitive[37] and may obscure dynamic, time-resolved changes, particularly those driven by transient regulators such as PERK[78]. To address this limitation, we implemented a single-time-point ISDia strategy, which enables temporal resolution of protein dynamics, albeit with reduced proteome depth. Together, these findings highlight ISDia as a versatile platform for protein dynamics analysis. Depending on the biological question, pooled, single-time-point, or full time-course designs can be strategically applied or integrated to optimize the balance between proteome coverage, quantitation robustness, and temporal resolution.

In summary, we developed ISDia, a streamlined and versatile proteomics platform, leveraging technological advancements in mass spectrometry to elucidate the regulation of protein dynamics during the UPR. We uncovered diverse regulatory mechanisms governing protein abundances by systematically and specifically modulating protein synthesis and clearance under stress conditions. These results highlight the potential of ISDia as a powerful tool for investigating protein dynamics in diverse stress contexts, including drug development and neurodegenerative disease models, and provide insights into the regulation of protein homeostasis during the UPR.

Limitations of the study

It is known that ER stress induces protein aggregation[6,79], and it is possible that the newly synthesized proteins are misfolded during the UPR and will undergo more rapid clearance. Coupling ISDia with differential buffers for protein extraction or strategies to barcode proteins based on their time of synthesis[80], could enable the separation of misfolded proteins to show how synthesis and clearance contributes to their accumulation, particularly under different genetic background or disease models.

Despite ISDia enabling protein dynamics analysis under non-steady states, it cannot be directly applied to clinical samples, as it requires the incorporation of isotope-labeled amino acids, as is possible in model systems, such as mouse and fly.

Elucidating mechanisms of protein synthesis and degradation regulation, such as identification of upstream E3 ligases, or defining the roles of proteins involved in the UPR, is beyond the scope of this study. To fully understand this mechanism, further studies are needed.

METHODS

Cell Culture and Isotope Labeling: Cells were cultured in DMEM supplemented with 10% fetal bovine serum (FBS) and 1% penicillin-streptomycin (P/S) at 37°C in a humidified incubator with 5% CO_2. For heavy isotope labeling, cells were gradually adapted to DMEM supplemented with 10% dialyzed FBS and 1% Penicillin-Streptomycin (P/S). For MS standards with pre-defined heavy/light (H/L) ratios, HCT116 cells were passaged seven times in SILAC DMEM supplemented with heavy isotope-labeled arginine (+10.008269 Da) and lysine (+8.014199 Da), 10% dialyzed FBS, and 1% P/S. Corresponding light control cells were cultured in SILAC DMEM with native arginine and lysine under identical conditions. Fully heavy isotope-labeled cells and light control cells were harvested separately and stored at -80°C for subsequent proteomics analysis.

To examine synthesis and clearance dynamics during the unfolded protein response (UPR), HeLa cells were treated with 2.5 µg/mL tunicamycin (Tm) and 200 nM thapsigargin (Th) for 0, 6, 12, 24, and 48 hours. Isotope labeling was initiated simultaneously using SILAC DMEM supplemented with heavy isotope-labeled arginine (+10.008269 Da) and lysine (+8.014199 Da), 10% dialyzed FBS, and 1% penicillin-streptomycin. DMSO-treated cells served as controls. Each condition was performed in triplicate. Following treatment, cells were harvested and stored at -80°C for proteomics analysis.

Western Blotting: Cells were harvested and lysed using RIPA buffer (25 mM Tris-HCl pH 7.6, 150 mM NaCl, 1% NP-40, 1% sodium deoxycholate, 0.1% SDS) supplemented with 1x protease inhibitor cocktail. Lysates were centrifuged at 14,000 rpm for 10 minutes at 4°C, and the supernatant was collected for protein quantification using the BCA assay. A total of 20 µg of protein per sample was used. Electrophoresis was performed at 200 V for 35 minutes using NuPAGE™ Bis-Tris gels. Proteins were transferred to PVDF membranes using the Invitrogen iBlot2 Gel Transfer Stacks (IB24001, 0.2 µm pore size). Membranes were then blocked for 1 hour at room temperature in 5% non-fat milk prepared in TBST buffer (20 mM Tris-HCl pH 8.0, 137 mM NaCl, 0.05% Tween-20). Membranes were incubated overnight at 4°C with the following primary antibodies: monoclonal rabbit anti-PERK (1:1000), anti-BiP (1:1000), anti-ATF4 (1:1000), anti-XBP1s (1:1000), and mouse anti-β-Actin (1:2500). Membranes were washed with TBST and incubated for 1 hour at room temperature with appropriate HRP-conjugated secondary antibodies: anti-rabbit IgG for rabbit primary antibodies or anti-mouse IgG for β-Actin. Protein bands were visualized using the Pierce™ Enhanced Chemiluminescence (ECL) detection system (Thermo Fisher Scientific) on a BioRad imager.

Sample preparation for proteomic analysis: Cell pellets were lysed in 8M urea, 200 mM EPPS, protease and phosphatase inhibitor (ThermoFisher Scientific) and sonicated. Then the supernatants were collected by centrifugation, and the protein concentrations were measured using Pierce BCA assay kits. Subsequently, proteins were reduced with 5 mM TCEP for 15 minutes, alkylated with 15 mM iodoacetamide in the dark for 30 minutes, and quenched with 10 mM DTT at room temperature. Next, 20 µg of protein was digested with LysC and trypsin overnight at 37°C with shaking at 1400 rpm on a ThermoMixer. Heavy and light samples were mixed at predefined H/L ratios of 1:1, 3:1, 9:1, and 27:1 prior to protein digestion, with three replicates per ratio. For ISDia, samples from the same treatment across four time points were pooled before digestion, also with three replicates per group. The samples were then desalted, dried and resuspended in 5% acetonitrile (ACN) and 5% formic acid (FA) for mass spectrometry analysis.

Liquid chromatography: LC was performed using a Vanquish Neo ultra high-performance liquid chromatography (UHPLC) system, configured in trap-and-elute format. Peptides were separated on an Aurora Frontier™ TS C18 UHPLC column (IonOpticks, 60 cm length, 75 µm inner diameter, 1.7 µm particle size). During LC separations, mobile phase A (MPA) was 0.1% formic acid (FA) in water and mobile phase B (MPB) was 80% ACN in water with 0.1% FA. A 50-min active gradient ramped, at a flow rate of 0.3 µl/min, from 12 to 18% MPB from 0.1 to 8 min, 18 to 45% MPB from 8 to 50 min at a flow rate of 0.2 µl/min, 45 to 99% MPB from 50 to 50.1min, and held at 99% MPB to 15 min before the column was washed and preequilibrated at 1% MPB for 35 min.

Mass spectrometry data acquisition: An Orbitrap Astral Mass Spectrometer was used for data acquisition, and equal amounts of sample were injected across all runs. In DDA methods, MS1 scans were collected in the Orbitrap with the resolution set to 120k, with the normalized AGC Target at 100%. The scan range was 350-1350 m/z, cycle time is 0.6s. For MS2 scans, precursor ion selection width was kept at 1.2 *m*/*z*. HCD collision energy was set to 25% with a maximum injection time 25 ms. Dynamic exclusion was enabled and set to 60 s.

For the DIA experiments, the Orbitrap Astral mass spectrometer was operated at a MS1 resolution of 240,000 with a full scan range of 380–980 *m/z*. The MS1 AGC was set to 250%. DIA scans were recorded at a resolution of 80,000 and maximum injection time of 2.5, 3.5, 4.5 or 5.5 ms. Isolation windows was set to 2 Th or 4 Th. HCD collison energy was set to 25%. For DIA method optimization, the Orbitrap Astral mass spectrometer was connected to the FAIMS pro interface at compensation voltage, -40V, -50 V, -55V, -60V, -65V were tested.

DDA data analysis: DDA raw files were analyzed using FragPipe (version 22.0) with the default SILAC3 workflow settings. Briefly, a human reference database (UniProt 2024/12/19 release, containing 83,401 entries) with concatenated and decoys was applied. In addition to the common variable and fixed modifications, heavy isotope modifications on R (+10.008269 Da) and K (+8.014199 Da) were designated as variable modifications for heavy-labeled peptides. Similarly, IonQuant was configured to run with SILAC light

and heavy labels and quantitation was based on the MS1 area, with intensities normalized across runs. PSM filtering was performed to a final protein-level FDR of 1%.

DIA data analysis: DIA raw files were searched using Spectronaut (version 19.6.250122.62635) with the default directDIA settings and the same database. For samples with heavy peptides, two-channel labeling was applied, with Channel 1 left unlabeled and Channel 2 labeled with “Arg10” and “Lys8”. Protein and peptide identifications were filtered to maintain a 1% FDR. Proteins were quantified based on the MS2 area. The “Exclude All Multi-Channel Interferences” option was enabled in Spectronaut to exclude interference from b ions in the same spectra.

Cellular compartment and protein complex analysis: Protein lists corresponding to different cellular compartments were obtained from UniProt based on Gene Ontology (GO) annotations. Annotations that mapped genes to protein complexes were obtained from Ori *et al.*[56], who compiled information from their own literature search, the CORUM protein complex database[81], and the COMPLEAT data resource[82]. We mapped ENSEMBL gene IDs from the annotated protein complexes to gene symbols, which were then mapped to the protein data.

Detecting treatment differences in protein complex-wide intensity: We first filtered the protein data to protein complexes with three or more subunits observed in the data to avoid making inferences based on only one or two proteins. We used linear mixed effects models (LMMs) to test for a treatment effect on intensity shared across complex subunits. For each protein complex, we fit the following joint model (Equation 4) of the complex’s annotated proteins for a given cell background and treatment:

$$\log_2(\text{intensity}_{ijk}) = \mu + \text{treatment}_{\text{T}}\mathrm{I}\{x_{ik}\} + \eta_j + \varepsilon_i \qquad (4)$$

where intensity_{ijk} is the intensity value for protein j of sample i exposed to treatment k, μ is a shared intercept, $\text{treatment}_{\text{T}}$ is the effect of treatment Tm or Th, $\mathrm{I}\{x_{ik}\}$ is an indicator function that sample i was exposed to treatment T, η_j is a random effect that allows for models protein-specific deviations from the overall complex, and ε_{ijk} is the unstructured random error term. The random terms are modeled as $\eta_j \sim \mathrm{N}(0, \tau^2)$ and $\varepsilon_i \sim \mathrm{N}(0, \sigma^2)$ where τ^2 and σ^2 are variance components. The treatment effect was tested with ANOVA by comparing the model in Eq1 to the null model excluding it. The LMMs were fit using the R package lme4[83]. Because our focus was testing, maximum likelihood estimation was used instead of restricted maximum likelihood (REML). Statistical significance was determined based on false discovery rate (FDR)-adjusted p-values, using the Benjamini-Hochberg method[84].

RESOURCE AVAILABILITY

Lead contact

Requests for further information and resources should be directed to and will be fulfilled by the lead contact, Tian Zhang (tian_zhang@virginia.edu).

Materials availability

This study did not generate new, unique reagents.

Data and code availability

- The mass spectrometry proteomics data generated in this study have been deposited to the ProteomeXchange Consortium via the PRIDE[85] partner repository with the dataset identifier PXD066472. Reviewer can access the dataset by logging in to the PRIDE website using the following account details: Username: reviewer_pxd066472@ebi.ac.uk Password: 2lv7idp1cTIh.

- All data processing and statistical analyses were conducted with the R statistical programming language[86]. All processed data and the R code used for statistical analyses and generating the reported findings are publicly available on GitHub (https://github.com/TianZhangLab/Code-for-Integral-Synthesis-and-clearance-analysis-via-DIA-ISDia). README file at the top of the directory provides description of directory contents, which includes an R script for generating each figure.

- Any additional information required to reanalyze the data reported in this paper is available from the lead contact upon request.

DECLARATION OF GENERATIVE AI AND AI-ASSISTED TECHNOLOGIES IN THE WRITING PROCESS

During the preparation of this work, the authors used ChatGPT in order to improve language and readability. After using this tool, the authors reviewed and edited the content as needed and take full responsibility for the content of the publication.

ACKNOWLDEGMENTS

We thank all members of the Zhang Lab for their active discussions and support. T.Z. was supported by NCI grant R00CA273170. J.A.P. was funded by NIH/NIGMS grants R01 GM132129 and R35 GM156406. We acknowledge funding support from the University of Virginia Comprehensive Cancer Center (UVACCC). We also thank Dr. Sina Ghaemmaghami from the Biology Department of University of Rochester, Dr. Luke Wiseman from the Department of Molecular and Cellular Biology at the Scripps Research, Drs. Chongzhi Zang, Yuh-Hwa Wang, Hui Li from the Department of Biochemistry and Molecular Genetics at the University of Virginia School of Medicine for their valuable suggestions and insightful discussion.

AUTHOR CONTRIBUTIONS

T.Z. conceptualized the project and designed the experiments. Y.D., D.K.Q, V. L., W. E. M., W. L., J.A.P. and T.Z. performed the experiments. Y.D. and T.Z. designed the methodology. J.Y. generated the structural model and performed structural analysis. Y.D., G.R.K. and T.Z. designed the statistical approach. Y.D., G.R.K. and T.Z. performed the analysis. Y.D., G.R.K., J.A.P., L.Q. and T.Z. wrote the manuscript. All authors reviewed the manuscript.

DECLARATION OF INTEREST

The authors declare no competing interests.

REFERENCES

1. Ross, A. B., Langer, J. D. & Jovanovic, M. Proteome Turnover in the Spotlight: Approaches, Applications, and Perspectives. *Molecular & Cellular Proteomics* **20**, 100016 (2021).
2. Buszczak, M., Signer, R. A. J. & Morrison, S. J. Cellular Differences in Protein Synthesis Regulate Tissue Homeostasis. *Cell* **159**, 242–251 (2014).
3. Yen, H.-C. S., Xu, Q., Chou, D. M., Zhao, Z. & Elledge, S. J. Global Protein Stability Profiling in Mammalian Cells. *Science* **322**, 918–923 (2008).
4. Uhlén, M. *et al.* Tissue-based map of the human proteome. *Science* **347**, 1260419 (2015).
5. Hetz, C., Zhang, K. & Kaufman, R. J. Mechanisms, regulation and functions of the unfolded protein response. *Nat Rev Mol Cell Biol* **21**, 421–438 (2020).
6. Walter, P. & Ron, D. The Unfolded Protein Response: From Stress Pathway to Homeostatic Regulation. *Science* **334**, 1081–1086 (2011).
7. Hwang, J. & Qi, L. Quality Control in the Endoplasmic Reticulum: Crosstalk between ERAD and UPR pathways. *Trends in Biochemical Sciences* **43**, 593–605 (2018).
8. Currie, J. *et al.* Simultaneous proteome localization and turnover analysis reveals spatiotemporal features of protein homeostasis disruptions. *Nat Commun* **15**, 2207 (2024).
9. Reich, S. *et al.* A multi-omics analysis reveals the unfolded protein response regulon and stress-induced resistance to folate-based antimetabolites. *Nat Commun* **11**, 2936 (2020).
10. Zhang, T., Shen, S., Qu, J. & Ghaemmaghami, S. Global Analysis of Cellular Protein Flux Quantifies the Selectivity of Basal Autophagy. *Cell Reports* **14**, 2426–2439 (2016).

11. Zhang, T. *et al.* Proteome-wide modulation of degradation dynamics in response to growth arrest. *Proc. Natl. Acad. Sci. U.S.A.* **114**, (2017).

12. Price, J. C., Guan, S., Burlingame, A., Prusiner, S. B. & Ghaemmaghami, S. Analysis of proteome dynamics in the mouse brain. *Proc. Natl. Acad. Sci. U.S.A.* **107**, 14508–14513 (2010).

13. Vogel, C. & Marcotte, E. M. Insights into the regulation of protein abundance from proteomic and transcriptomic analyses. *Nat Rev Genet* **13**, 227–232 (2012).

14. Li, W. *et al.* Turnover atlas of proteome and phosphoproteome across mouse tissues and brain regions. *Cell* **188**, 2267-2287.e21 (2025).

15. Sabatier, P. *et al.* Global analysis of protein turnover dynamics in single cells. *Cell* **188**, 2433-2450.e21 (2025).

16. Ong, S.-E. *et al.* Stable Isotope Labeling by Amino Acids in Cell Culture, SILAC, as a Simple and Accurate Approach to Expression Proteomics. *Molecular & Cellular Proteomics* **1**, 376–386 (2002).

17. Alevra, M. *et al.* A mass spectrometry workflow for measuring protein turnover rates in vivo. *Nat Protoc* **14**, 3333–3365 (2019).

18. Welle, K. A. *et al.* Time-resolved Analysis of Proteome Dynamics by Tandem Mass Tags and Stable Isotope Labeling in Cell Culture (TMT-SILAC) Hyperplexing. *Molecular & Cellular Proteomics* **15**, 3551–3563 (2016).

19. Savitski, M. M. *et al.* Multiplexed Proteome Dynamics Profiling Reveals Mechanisms Controlling Protein Homeostasis. *Cell* **173**, 260-274.e25 (2018).

20. Li, J. *et al.* TMTpro reagents: a set of isobaric labeling mass tags enables simultaneous proteome-wide measurements across 16 samples. *Nat Methods* **17**, 399–404 (2020).

21. Guzman, U. H. *et al.* Ultra-fast label-free quantification and comprehensive proteome coverage with narrow-window data-independent acquisition. *Nat Biotechnol* (2024) doi:10.1038/s41587-023-02099-7.

22. Hinkson, I. V. & Elias, J. E. The dynamic state of protein turnover: It's about time. *Trends in Cell Biology* **21**, 293–303 (2011).

23. Fröhlich, K. *et al.* Data-Independent Acquisition: A Milestone and Prospect in Clinical Mass Spectrometry–Based Proteomics. *Molecular & Cellular Proteomics* **23**, 100800 (2024).

24. Pino, L. K., Baeza, J., Lauman, R., Schilling, B. & Garcia, B. A. Improved SILAC Quantification with Data-Independent Acquisition to Investigate Bortezomib-Induced Protein Degradation. *J. Proteome Res.* **20**, 1918–1927 (2021).

25. Salovska, B. *et al.* A robust multiplex-DIA workflow profiles protein turnover regulations associated with cisplatin resistance and aneuploidy. *Nat Commun* **16**, 5034 (2025).

26. Stewart, H. *et al.* A Conjoined Rectilinear Collision Cell and Pulsed Extraction Ion Trap with Auxiliary DC Electrodes. *J Am Soc Mass Spectrom* **35**, 74–81 (2024).

27. Grinfeld, D. *et al.* Multi-reflection Astral mass spectrometer with isochronous drift in elongated ion mirrors. *Nuclear Instruments and Methods in Physics Research Section A: Accelerators, Spectrometers, Detectors and Associated Equipment* **1060**, 169017 (2024).

28. Li, J., Smith, L. S. & Zhu, H.-J. Data-independent acquisition (DIA): An emerging proteomics technology for analysis of drug-metabolizing enzymes and transporters. *Drug Discovery Today: Technologies* **39**, 49–56 (2021).

29. Serrano, L. R. *et al.* The One Hour Human Proteome. *Mol Cell Proteomics* **23**, 100760 (2024).

30. Keele, G. R. *et al.* Expanding the landscape of aging via orbitrap astral mass spectrometry and tandem mass tag integration. *Nat Commun* **16**, 4753 (2025).

31. Sharma, K. *et al.* Ultradeep Human Phosphoproteome Reveals a Distinct Regulatory Nature of Tyr and Ser/Thr-Based Signaling. *Cell Reports* **8**, 1583–1594 (2014).

32. Li, W., Salovska, B., Fornasiero, E. F. & Liu, Y. Toward a hypothesis-free understanding of how phosphorylation dynamically impacts protein turnover. *Proteomics* **23**, 2100387 (2023).

33. Salovska, B. *et al.* Isoform-resolved correlation analysis between mRNA abundance regulation and protein level degradation. *Mol Syst Biol* **16**, e9170 (2020).

34. Zhang, T., Gygi, S. P. & Paulo, J. A. Temporal Proteomic Profiling of SH-SY5Y Differentiation with Retinoic Acid Using FAIMS and Real-Time Searching. *J Proteome Res* **20**, 704–714 (2021).

35. Schweppe, D. K. *et al.* Characterization and Optimization of Multiplexed Quantitative Analyses Using High-Field Asymmetric-Waveform Ion Mobility Mass Spectrometry. *Anal. Chem.* **91**, 4010–4016 (2019).

36. Gaetani, M. *et al.* Proteome Integral Solubility Alteration: A High-Throughput Proteomics Assay for Target Deconvolution. *J. Proteome Res.* **18**, 4027–4037 (2019).

37. Mateus, A. *et al.* Thermal proteome profiling for interrogating protein interactions. *Molecular Systems Biology* **16**, (2020).

38. Bertolotti, A., Zhang, Y., Hendershot, L. M., Harding, H. P. & Ron, D. Dynamic interaction of BiP and ER stress transducers in the unfolded-protein response. *Nat Cell Biol* **2**, 326–332 (2000).

39. Kopp, M. C., Larburu, N., Durairaj, V., Adams, C. J. & Ali, M. M. U. UPR proteins IRE1 and PERK switch BiP from chaperone to ER stress sensor. *Nat Struct Mol Biol* **26**, 1053–1062 (2019).

40. Harding, H. P. *et al.* An Integrated Stress Response Regulates Amino Acid Metabolism and Resistance to Oxidative Stress. *Molecular Cell* **11**, 619–633 (2003).

41. Han, J. *et al.* ER-stress-induced transcriptional regulation increases protein synthesis leading to cell death. *Nat Cell Biol* **15**, 481–490 (2013).

42. Brewer, J. W. & Diehl, J. A. PERK mediates cell-cycle exit during the mammalian unfolded protein response. *Proc. Natl. Acad. Sci. U.S.A.* **97**, 12625–12630 (2000).

43. Hamanaka, R. B., Bennett, B. S., Cullinan, S. B. & Diehl, J. A. PERK and GCN2 Contribute to eIF2α Phosphorylation and Cell Cycle Arrest after Activation of the Unfolded Protein Response Pathway. *MBoC* **16**, 5493–5501 (2005).

44. Lemberg, M. K. & Strisovsky, K. Maintenance of organellar protein homeostasis by ER-associated degradation and related mechanisms. *Molecular Cell* **81**, 2507–2519 (2021).

45. Mårtensson, C. U. *et al.* Mitochondrial protein translocation-associated degradation. *Nature* **569**, 679–683 (2019).

46. Tsai, P.-L. *et al.* Dynamic quality control machinery that operates across compartmental borders mediates the degradation of mammalian nuclear membrane proteins. *Cell Reports* **41**, 111675 (2022).

47. Rousseau, A. & Bertolotti, A. Regulation of proteasome assembly and activity in health and disease. *Nat Rev Mol Cell Biol* **19**, 697–712 (2018).

48. Filbeck, S., Cerullo, F., Pfeffer, S. & Joazeiro, C. A. P. Ribosome-associated quality-control mechanisms from bacteria to humans. *Molecular Cell* **82**, 1451–1466 (2022).

49. Pihán, P., Ellerby, L. M. & Hetz, C. ER–mitochondria contact sites: a refuge for mitochondrial mRNAs under ER stress. *Trends in Cell Biology* S0962892425000364 (2025) doi:10.1016/j.tcb.2025.02.002.

50. Brar, K. K. *et al.* PERK-ATAD3A interaction provides a subcellular safe haven for protein synthesis during ER stress. *Science* **385**, eadp7114 (2024).

51. Itoh, K., Tamura, Y., Iijima, M. & Sesaki, H. Effects of Fcj1-Mos1 and mitochondrial division on aggregation of mitochondrial DNA nucleoids and organelle morphology. *MBoC* **24**, 1842–1851 (2013).

52. Ban-Ishihara, R., Ishihara, T., Sasaki, N., Mihara, K. & Ishihara, N. Dynamics of nucleoid structure regulated by mitochondrial fission contributes to cristae reformation and release of cytochrome *c*. *Proc. Natl. Acad. Sci. U.S.A.* **110**, 11863–11868 (2013).

53. Ishihara, T. *et al.* Dynamics of Mitochondrial DNA Nucleoids Regulated by Mitochondrial Fission Is Essential for Maintenance of Homogeneously Active Mitochondria during Neonatal Heart Development. *Molecular and Cellular Biology* **35**, 211–223 (2015).

54. Dörig, C. *et al.* Global profiling of protein complex dynamics with an experimental library of protein interaction markers. *Nat Biotechnol* (2024) doi:10.1038/s41587-024-02432-8.

55. Mathieson, T. *et al.* Systematic analysis of protein turnover in primary cells. *Nat Commun* **9**, 689 (2018).

56. Ori, A. *et al.* Spatiotemporal variation of mammalian protein complex stoichiometries. *Genome Biol* **17**, 47 (2016).

57. Dudek, J., Guiard, B. & Rehling, P. The Role of the TIM23 Complex and Its Associated Motor Complex in Mitochondrial Protein Import. in *The Enzymes* vol. 25 387–411 (Elsevier, 2007).

58. Schulz, C. *et al.* Tim50's presequence receptor domain is essential for signal driven transport across the TIM23 complex. *Journal of Cell Biology* **195**, 643–656 (2011).

59. Schmidt, O., Pfanner, N. & Meisinger, C. Mitochondrial protein import: from proteomics to functional mechanisms. *Nat Rev Mol Cell Biol* **11**, 655–667 (2010).

60. Sun, Z. & Brodsky, J. L. Protein quality control in the secretory pathway. *Journal of Cell Biology* **218**, 3171–3187 (2019).

61. Wang, H. H., Biunno, I., Sun, S. & Qi, L. SEL1L–HRD1-mediated ERAD in mammals. *Nat Cell Biol* (2025) doi:10.1038/s41556-025-01690-1.

62. Lee, A.-H., Iwakoshi, N. N. & Glimcher, L. H. XBP-1 Regulates a Subset of Endoplasmic Reticulum Resident Chaperone Genes in the Unfolded Protein Response. *Molecular and Cellular Biology* **23**, 7448–7459 (2003).

63. Adachi, Y. *et al.* ATF6 Is a Transcription Factor Specializing in the Regulation of Quality Control Proteins in the Endoplasmic Reticulum. *Cell Struct. Funct.* **33**, 75–89 (2008).

64. Cox, J. S., Shamu, C. E. & Walter, P. Transcriptional induction of genes encoding endoplasmic reticulum resident proteins requires a transmembrane protein kinase. *Cell* **73**, 1197–1206 (1993).

65. Yamamoto, K. Differential Contributions of ATF6 and XBP1 to the Activation of Endoplasmic Reticulum Stress-Responsive cis-Acting Elements ERSE, UPRE and ERSE-II. *Journal of Biochemistry* **136**, 343–350 (2004).

66. Rao, B. *et al.* The cryo-EM structure of an ERAD protein channel formed by tetrameric human Derlin-1. *Sci. Adv.* **7**, eabe8591 (2021).

67. Ye, Y., Shibata, Y., Yun, C., Ron, D. & Rapoport, T. A. A membrane protein complex mediates retro-translocation from the ER lumen into the cytosol. *Nature* **429**, 841–847 (2004).

68. Abramson, J. *et al.* Accurate structure prediction of biomolecular interactions with AlphaFold 3. *Nature* **630**, 493–500 (2024).

69. Van Den Boom, J., Marini, G., Meyer, H. & Saibil, H. R. Structural basis of ubiquitin-independent PP1 complex disassembly by p97. *The EMBO Journal* **42**, e113110 (2023).

70. Zhu, K. *et al.* The phosphorylation and dephosphorylation switch of VCP/p97 regulates the architecture of centrosome and spindle. *Cell Death Differ* **29**, 2070–2088 (2022).

71. Meyer, H., Bug, M. & Bremer, S. Emerging functions of the VCP/p97 AAA-ATPase in the ubiquitin system. *Nat Cell Biol* **14**, 117–123 (2012).

72. Meyer, H. & Weihl, C. C. The VCP/p97 system at a glance: connecting cellular function to disease pathogenesis. *Journal of Cell Science* jcs.093831 (2014) doi:10.1242/jcs.093831.

73. Rohrer, J. D. *et al.* A novel exon 2 I27V VCP variant is associated with dissimilar clinical syndromes. *J Neurol* **258**, 1494–1496 (2011).

74. Bortel, P. *et al.* Systematic Optimization of Automated Phosphopeptide Enrichment for High-Sensitivity Phosphoproteomics. *Molecular & Cellular Proteomics* **23**, 100754 (2024).

75. Mitchell, D. C. *et al.* A proteome-wide atlas of drug mechanism of action. *Nat Biotechnol* **41**, 845–857 (2023).

76. Rainbolt, T. K., Atanassova, N., Genereux, J. C. & Wiseman, R. L. Stress-Regulated Translational Attenuation Adapts Mitochondrial Protein Import through Tim17A Degradation. *Cell Metabolism* **18**, 908–919 (2013).

77. Hsu, M.-C. *et al.* Mitochondrial YME1L1 governs unoccupied protein translocase channels. *Nat Cell Biol* **27**, 309–321 (2025).

78. Perea, V. *et al.* PERK signaling promotes mitochondrial elongation by remodeling membrane phosphatidic acid. *EMBO J* **42**, e113908 (2023).

79. Chen, X., Shi, C., He, M., Xiong, S. & Xia, X. Endoplasmic reticulum stress: molecular mechanism and therapeutic targets. *Sig Transduct Target Ther* **8**, 352 (2023).

80. Meadow, M. E. *et al.* Proteome Birthdating Reveals Age-Selectivity of Protein Ubiquitination. *Molecular & Cellular Proteomics* **23**, 100791 (2024).

81. Tsitsiridis, G. *et al.* CORUM: the comprehensive resource of mammalian protein complexes-2022. *Nucleic Acids Res* **51**, D539–D545 (2023).

82. Vinayagam, A. *et al.* Protein complex-based analysis framework for high-throughput data sets. *Sci Signal* **6**, rs5 (2013).

83. Bates, D., Mächler, M., Bolker, B. & Walker, S. Fitting Linear Mixed-Effects Models Using **lme4**. *J. Stat. Soft.* **67**, (2015).

84. Benjamini, Y. & Hochberg, Y. Controlling the False Discovery Rate: A Practical and Powerful Approach to Multiple Testing. *Journal of the Royal Statistical Society Series B: Statistical Methodology* **57**, 289–300 (1995).

85. Deutsch, E. W. *et al.* The ProteomeXchange consortium at 10 years: 2023 update. *Nucleic Acids Research* **51**, D1539–D1548 (2023).

86. R Core Team. *R: A Language and Environment for Statistical Computing*. (R Foundation for Statistical Computing, Vienna, Austria, 2023).

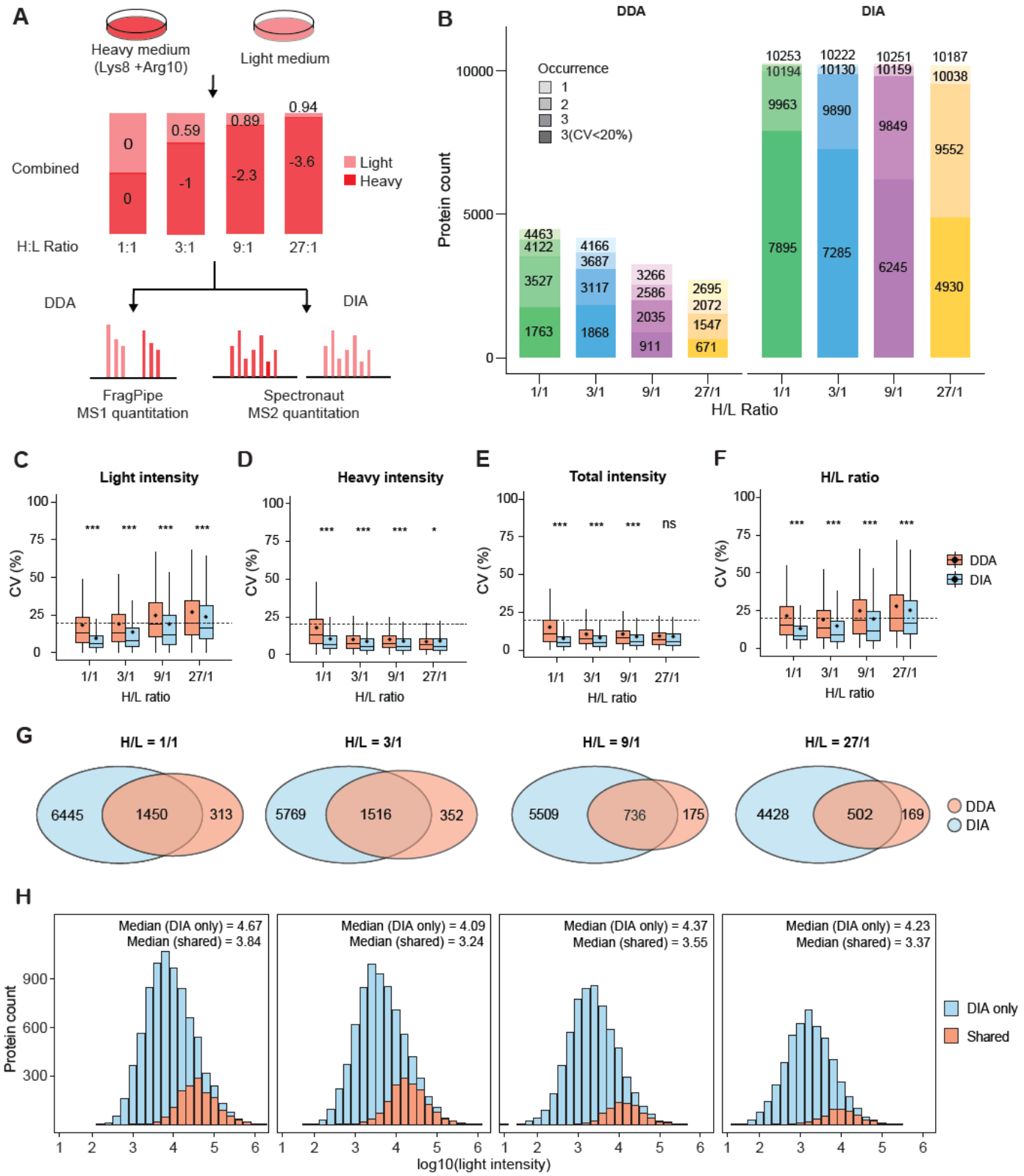

Figure 1. DIA on Orbitrap Astral mass spectrometer improves proteome coverage of pSILAC.

(A) Workflow for generating standards with pre-defined H/L ratios. Light and heavy intensities were normalized to those from the 1:1 standard sample. Resulting ratios are shown as $\log_2$-transformed fold changes.

(B) Proteome coverage achieved by DDA and DIA methods across standards. Each bar shows four numbers representing the number of proteins for which both light and heavy intensities were detected

in one, two, or all three replicates, or were consistently quantified across all three replicates with a coefficient of variation (CV) < 20% for light, heavy, total intensities, and H/L ratios.

(C) Boxplots showing the CV of light peptide intensities across replicates of the standards. The black dashed line indicates the 20% CV threshold. Statistical comparisons were performed using two-sided unpaired t-tests. *** $p < 0.001$; ** $0.001 < p < 0.01$; * $0.01 < p < 0.05$; ns $p > 0.05$.

(D) Boxplots showing the CV of heavy peptide intensities across replicates of the standards.

(E) Boxplots showing the CV of H/L ratios across replicates of the standards.

(F) Boxplots showing the CV of total intensity across replicates of the standards.

(G) Venn diagram showing the overlap of proteins quantified by DIA and DDA analysis of the standards. Only proteins with CV less than 20% for light, heavy, total intensities, and H/L ratios were included.

(H) Light peptide intensities in DIA for proteins quantified by both DIA and DDA, compared to those quantified exclusively by DIA analysis of the standards. The median light intensities for the two groups were labeled.

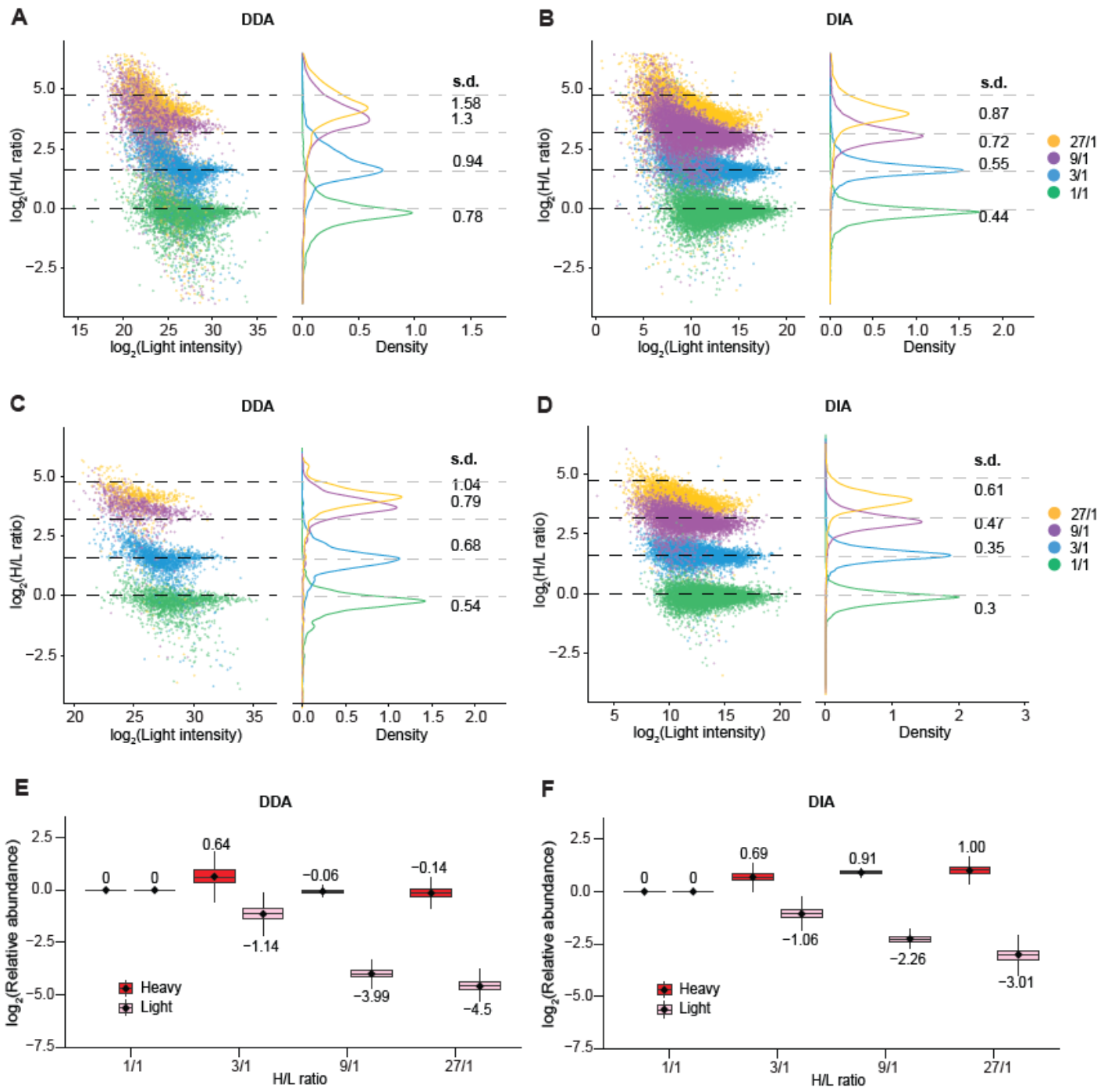

Figure 2. DIA enhanced quantitation accuracy within and across standards

(A) Scatter and density plots of light intensities for proteins quantified by DDA analysis of the standards. s.d. indicates the standard deviation of $\log_2$(H/L) ratios within each group; Dashed lines mark theoretical $\log_2$(H/L) values: $\log_2(1) = 0$, $\log_2(3) = 1.58$, $\log_2(9) = 3.17$, and $\log_2(27) = 4.75$.

(B) Same plot as in (A), showing light intensities as measured by DIA analysis.

(C) Same plot as in (A), showing light intensities measured by DDA analysis and filtered using CV < 20% for light, heavy, total intensity, and H/L ratio; CVs were calculated when the protein is quantified in all three replicates.

(D) Same plot as in (C), showing light intensities as measured by DIA analysis.

(E) Quantification of light and heavy peptide intensities in standards by DDA. Light and heavy intensities were normalized to those from the 1:1 standard sample. Theoretical log_2-transformed fold changes were labeled in Fig. 1A. Only proteins with CV < 20% for light, heavy, total intensities, and H/L ratios were included. Each dot and corresponding value represent the mean of measurements. Theoretical ratios were indicated in Fig. 1A.

(F) Same plot as in (E), showing DIA data.

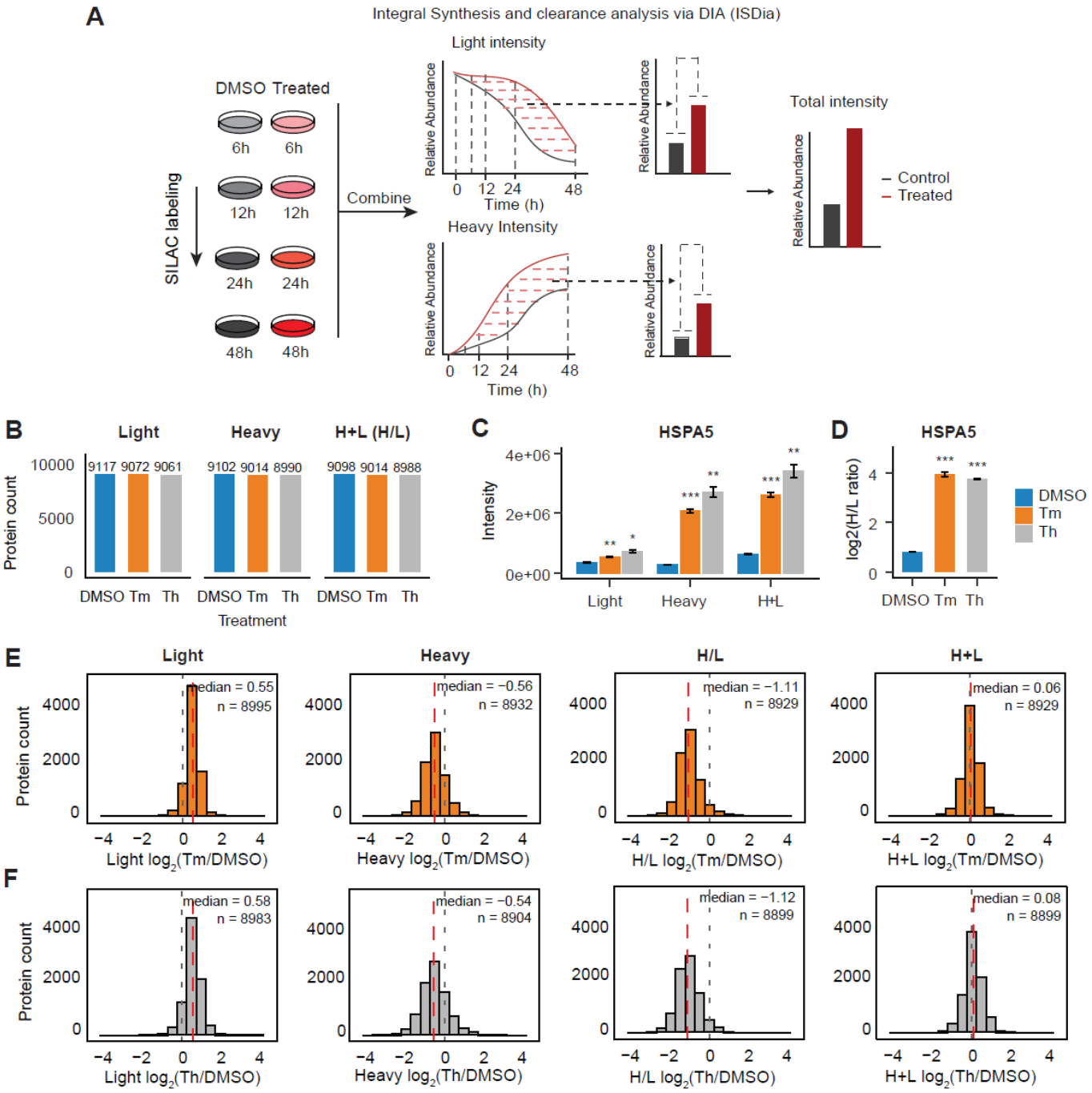

Figure 3. Development of ISDia with a streamlined workflow and increased proteome coverage

(A) ISDia workflow.

(B) Number of proteins quantified with light, heavy, and H+L intensities (H/L ratio) across all three replicates, respectively. H+L and H/L ratio values are included only when both light and heavy intensities were quantified.

(C) Changes in light, heavy, and H+L intensities of HSPA5 upon Th and Tm treatment compared to DMSO. Statistical significance: *** $p < 0.001$; ** $0.001 < p < 0.01$; * $0.01 < p < 0.05$.

(D) Log2(H/L ratio) changes of HSPA5 upon Th and Tm treatment compared to DMSO. Significance is indicated as in (C).

(E) Distribution of $\log_2$ fold changes for light, heavy, H/L ratio and H+L intensity under Tm treatment relative to DMSO. H+L intensity and H/L ratio values were included only when both light and heavy intensity quantitation were available. *n* indicates the number of proteins included in each panel.

(F) Same plot as in (E), showing data under Th treatment relative to DMSO.

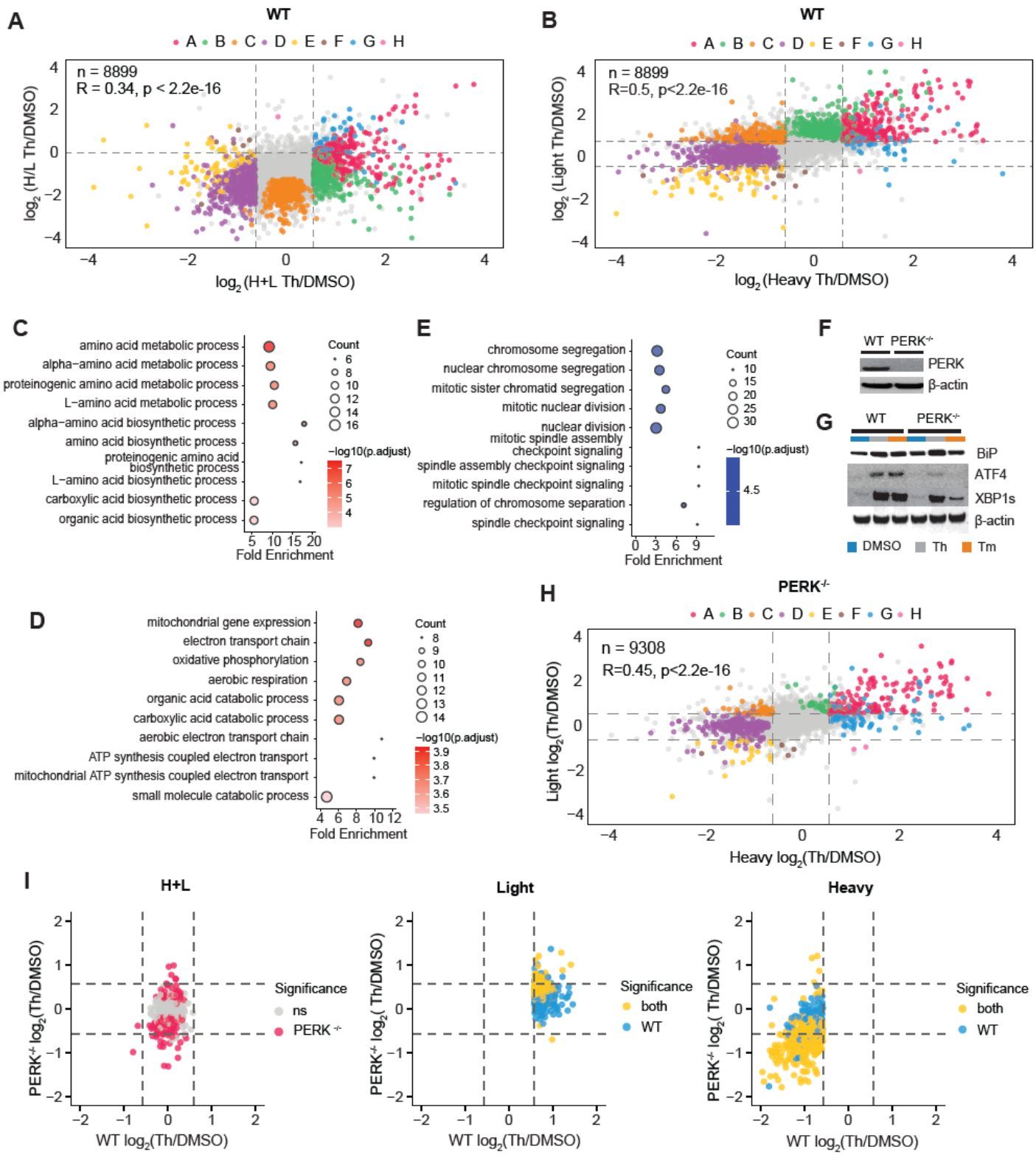

Figure 4. Coordination of protein synthesis and clearance modulates proteome dynamics during the UPR

(A) Pairwise comparison of changes in H+L and H/L ratio between Th and DMSO treatments. Each point represents a protein. Grey dashed lines indicate the fold change threshold of $\log_2(1.5) \approx \pm 0.58$ for H+L, and $\log_2(1) = 0$ indicating no change for H/L ratio. Proteins are color-coded based on their changes across light,

heavy, and H+L as follows: dark pink (up in light, heavy, and H+L); green (up in light and H+L, heavy not significant); orange (light up, heavy down, H+L not significant); purple (down in heavy and H+L, light not significant); yellow (down in light, heavy, and H+L); brown (down in light and H+L, heavy not significant); blue (up in heavy and H+L, light not significant); light pink (light down, heavy up, H+L not significant); grey (others). Up is FC > 0.58 & p-value < 0.05; Down is FC < -0.58 & p-value < 0.05. n is the number of proteins shown; R is the Pearson correlation coefficient; p is the corresponding p-value.

(B) Pairwise comparison of changes in heavy and light intensities under Th and DMSO treatment. Color scheme and significance thresholds are the same as (A).

(C) Biological processes enriched among the proteins with upregulated light, heavy intensities and increased H+L, H/L under Th treatment compared to DMSO.

(D) Biological processes enriched among the proteins with upregulated light, heavy and decreased H+L, H/L under Th treatment compared to DMSO.

(E) Biological processes enriched among the proteins with downregulated heavy and no upregulated light intensities under Th treatment (purple and yellow in (A) and (B)).

(F) Western blotting analysis showing the expression of PERK in WT and PERK$^{-/-}$ cells.

(G) Western blotting analysis showing the downstream factor levels after cells were treated with 2.5 μg/mL tunicamycin (Tm) and 200 nM thapsigargin (Th) for 6 hours in WT and PERK$^{-/-}$ cells.

(H) Pairwise comparison of changes in heavy and light intensities changes under Th and DMSO treatment in PERK$^{-/-}$ cells. Color scheme and significance thresholds are the same as (A).

(I) Pairwise comparison of the log2 fold change in H+L, heavy and light intensity under Th treatment relative to DMSO in WT and PERK$^{-/-}$ cells.

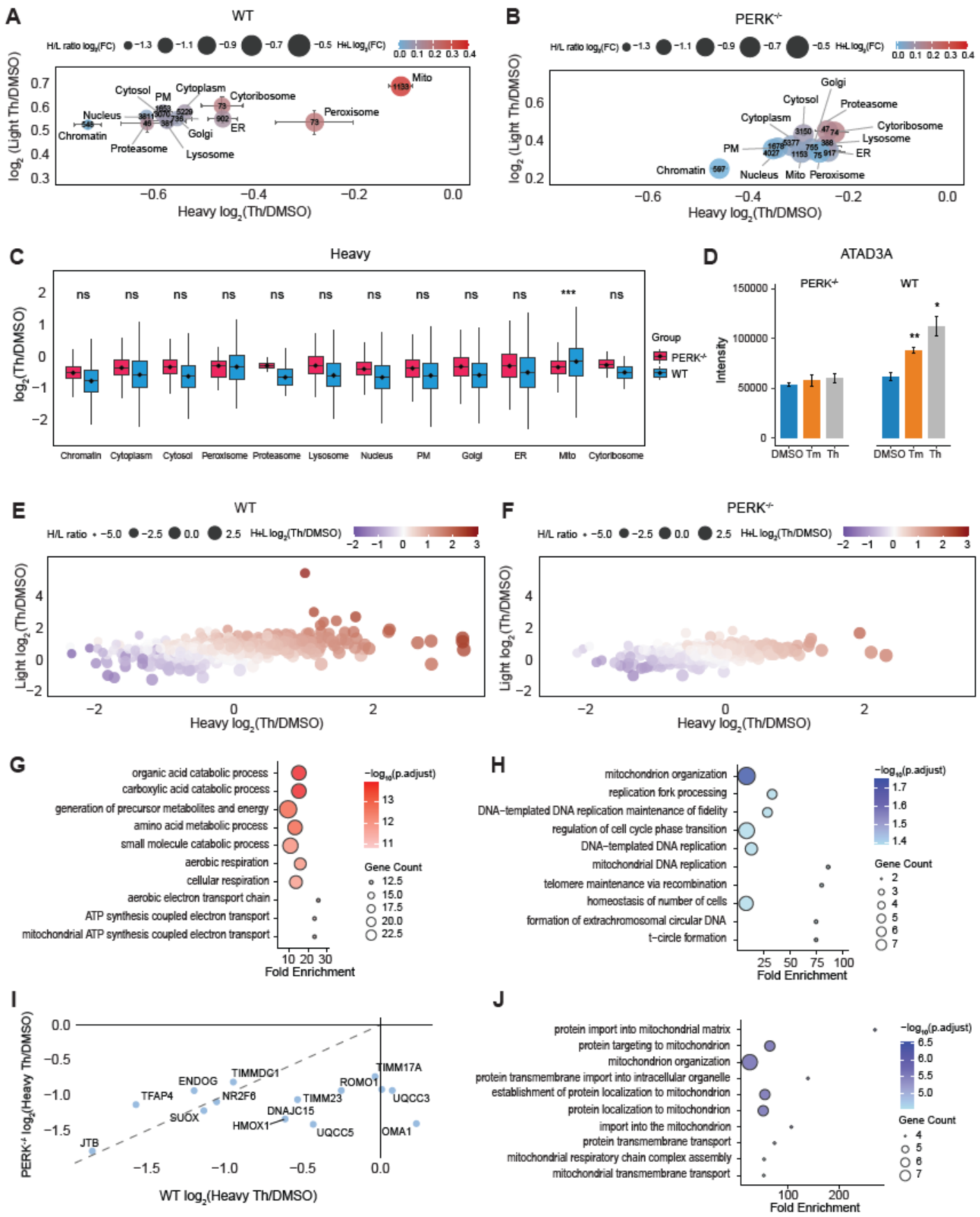

Figure 5. Differential regulation of protein synthesis and clearance across cellular compartments during the UPR

(A) Bubble plots showing the median of log_2(Th/DMSO) changes in light, heavy, H+L, and H/L ratio across subcellular compartments in WT cells. Values indicate the number of proteins per compartment. Error bars represent ± the standard deviation of the median.

(B) Same plot as in (A), showing data in PERK$^{-/-}$ cells.

(C) Boxplot of log_2(Th/DMSO) fold changes in heavy peptide intensities comparing WT and PERK$^{-/-}$ cells across subcellular compartments. P-values are from paired, one-tailed t-tests. *** $p < 0.001$; ** $0.001 < p < 0.01$; * $0.01 < p < 0.05$; ns, $p > 0.05$.

(D) H+L intensity changes of ATAD3A in WT and PERK$^{-/-}$ cells under DMSO, Th and Tm treatments. *** $p < 0.001$; ** $0.001 < p < 0.01$; * $0.01 < p < 0.05$.

(E) Bubble plots showing log_2(Th/DMSO) changes in light, heavy, H+L, and H/L ratios, for mitochondrial proteins in WT cells.

(F) Same plot as in (E), showing data in PERK$^{-/-}$ cells.

(G) Biological processes enriched among the mitochondrial proteins with potential increased protein synthesis (Heavy log_2(Th/DMSO) > 0.58 & p-value < 0.05; L log_2(Th/DMSO) > 0.58 & p-value < 0.05; H/L log_2(Th/DMSO) > 0) in WT cells.

(H) Biological processes enriched among the mitochondrial proteins with potential decreased protein synthesis (Heavy log_2(Th/DMSO) < -0.58 & p-value < 0.05; H+L log_2(Th/DMSO) < -0.58 & p-value < 0.05; H/L log_2(Th/DMSO) < 0 but not Light log_2(Th/DMSO) < -0.58 & p-value < 0.05) in WT cells.

(I) Scatter plot showing log_2(Th/DMSO) changes in heavy peptide intensity in WT and PERK$^{-/-}$ cells for mitochondrial proteins with potential decreased synthesis (Heavy log_2(Th/DMSO) < -0.58 & p-value < 0.05; H+L log_2(Th/DMSO) < -0.58 & p-value < 0.05; H/L log_2(Th/DMSO) < 0 but not Light log_2(Th/DMSO) < -0.58 & p-value < 0.05) in PERK$^{-/-}$ cells.

(J) Biological processes enriched among proteins in (I).

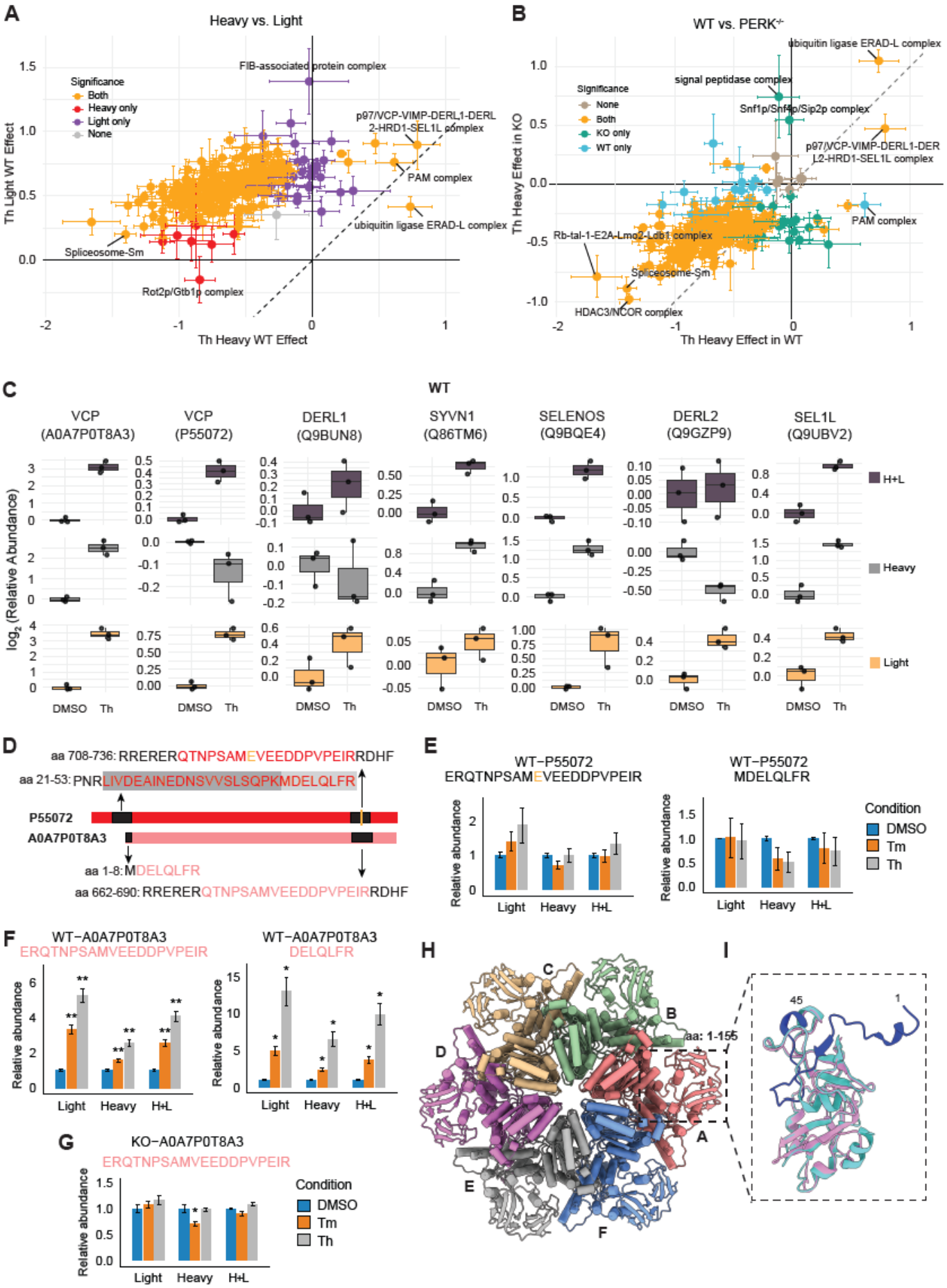
A
Heavy vs. Light
Significance
Both
Heavy only
Light only
None
FIB-associated protein complex
p97/VCP-VIMP-DERL1-DERL2-HRD1-SEL1L complex
PAM complex
ubiquitin ligase ERAD-L complex
Spliceosome-Sm
Rot2p/Gtb1p complex
Th Light WT Effect
Th Heavy WT Effect
B
WT vs. PERK-/-
ubiquitin ligase ERAD-L complex
signal peptidase complex
Snf1p/Snf4p/Sip2p complex
p97/VCP-VIMP-DERL1-DERL2-HRD1-SEL1L complex
PAM complex
Rb-tal-1-E2A-Lmo2-Ldb1 complex
Spliceosome-Sm
HDAC3/NCOR complex
Th Heavy Effect in KO
Th Heavy Effect in WT
C
WT
VCP (A0A7P0T8A3)
VCP (P55072)
DERL1 (Q9BUN8)
SYVN1 (Q86TM6)
SELENOS (Q9BQE4)
DERL2 (Q9GZP9)
SEL1L (Q9UBV2)
log2 (Relative Abundance)
H+L
Heavy
Light
DMSO
Th
D
aa 708-736: RRERERQTNPSAMEVEEDDPVPEIRRDHF
aa 21-53: PNRLIVDEAINEDNSVVSLSQPKMDELQLFR
P55072
A0A7P0T8A3
aa 1-8: MDELQLFR
aa 662-690: RRERERQTNPSAMVEEDDPVPEIRRDHF
E
WT−P55072
ERQTNPSAMEVEEDDPVPEIR
WT−P55072
MDELQLFR
Relative abundance
Light
Heavy
H+L
Condition
DMSO
Tm
Th
F
WT−A0A7P0T8A3
ERQTNPSAMVEEDDPVPEIR
WT−A0A7P0T8A3
DELQLFR
Relative abundance
Light
Heavy
H+L
G
KO−A0A7P0T8A3
ERQTNPSAMVEEDDPVPEIR
Relative abundance
Light
Heavy
H+L
Condition
DMSO
Tm
Th
H
A
B
C
D
E
F
aa: 1-155
I
45
1

Figure 6. Dynamic control of synthesis and clearance across protein complex subunits during the UPR

(A) Pairwise comparison of changes in heavy and light peptide intensities of protein complexes in WT cells treated with Th relative to DMSO.

(B) Pairwise comparison of changes in heavy peptide intensities of protein complexes under Th treatment relative to DMSO in WT and PERK$^{-/-}$ cells.

(C) Boxplot of changes of H+L, heavy and light intensities under Th treatment relative to DMSO for subunits of the p97/VCP-VIMP-DERL1-DERL2-HRD1-SEL1L complex in WT cells.

(D) Isoform-specific peptides in two p97/VCP isoforms.

(E) Bar plot showing the relative abundance of long p97/VCP isoform-specific (UniProt ID: P55072), peptides under DMSO and Th, Tm treatments in WT cells.

(F) Same plots as in (E) for short p97/VCP isoform-specific (UniProt ID: A0AP0T8A3) peptides in WT cells.

(G) Bar plots showing the relative intensity of short-isoform specific peptide under DMSO, Th and Tm treatments in PERK$^{-/-}$ cells.

(H) AlphaFold3-predicted hexameric model of the short p97/VCP isoform (UniProt ID: A0AP0T8A3), shown in top-down view with each protomer colored distinctly (labeled A-F). The region corresponding to residues 1-155 of the short isoform is indicated.

(I) Structural alignment of the N-terminal domains of the short isoform (pink, residues 1-155) and long isoform (cyan, residues 1-200), highlighting the additional N-terminal extension (residues 1-45, dark blue) present only in the long isoform. This extension includes the first β-strand that contributes to a β-sheet, potentially stabilizing the overall N-terminal fold.

A

Setting	In-silico generate missing channels	Multi channel workflow definition	Cross-run normalization
1	X	From library annotation	√ (direct DIA default)
2	Label	From library annotation	√ (direct DIA default)
3	X	Spike-in (Reference-based identification)	√ (direct DIA default)
4	Label	Spike-in (Reference-based identification)	√ (direct DIA default)
5	X	From library annotation	X

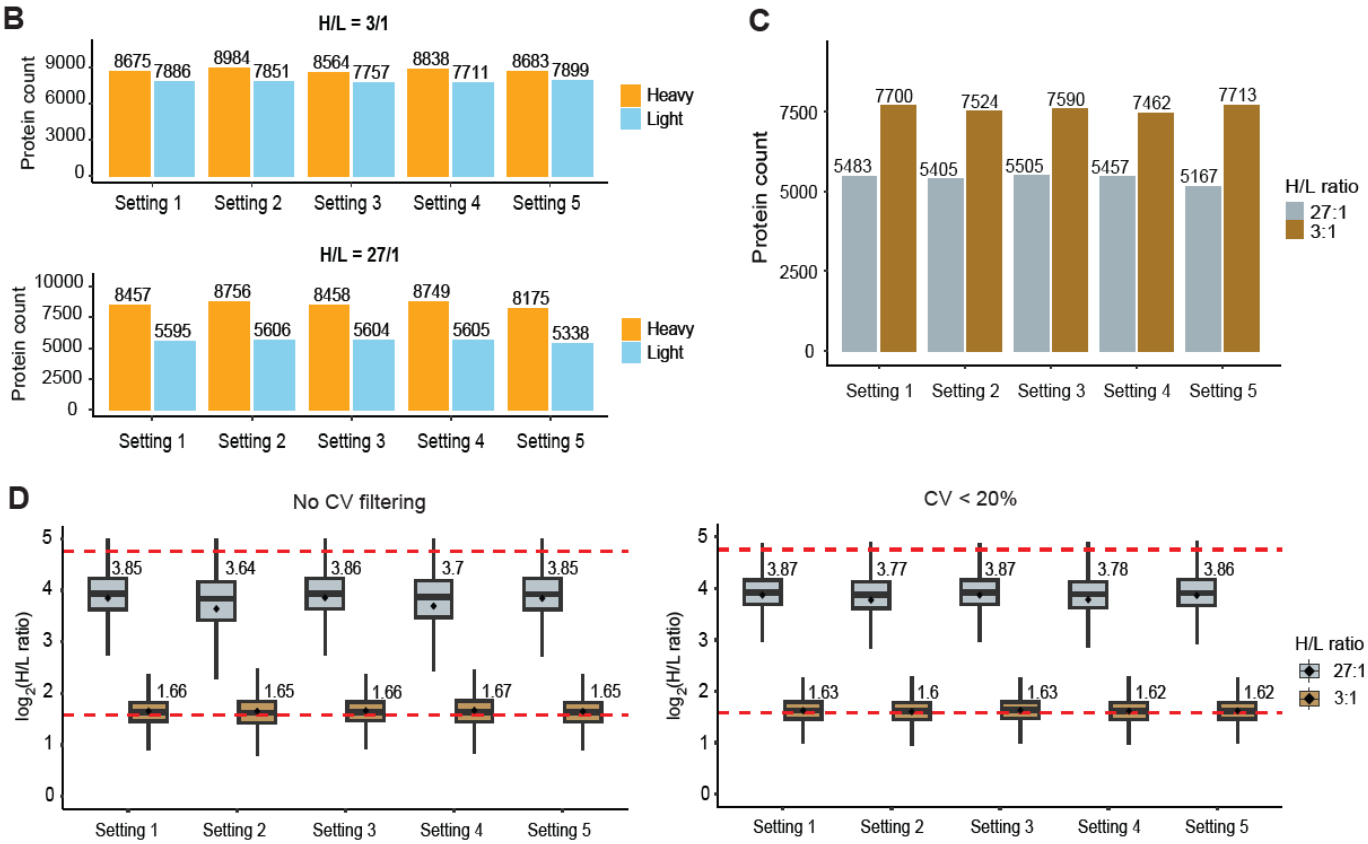

Figure S1. Testing Spectronaut search setting parameters, related to Figure 1.

(A) Table of Spectronaut settings tested.

(B) Number of proteins quantified with CV < 20% for either heavy or light peptide intensities across different settings. CVs were calculated when the protein is quantified in all three replicates.

(C) Number of proteins quantified with CV < 20% for either heavy or light peptide intensities across different settings.

(D) $\log_2$(H/L ratio) across different settings with or without filtering by CV < 20% for both heavy and light channels in standards with pre-defined H/L ratios.

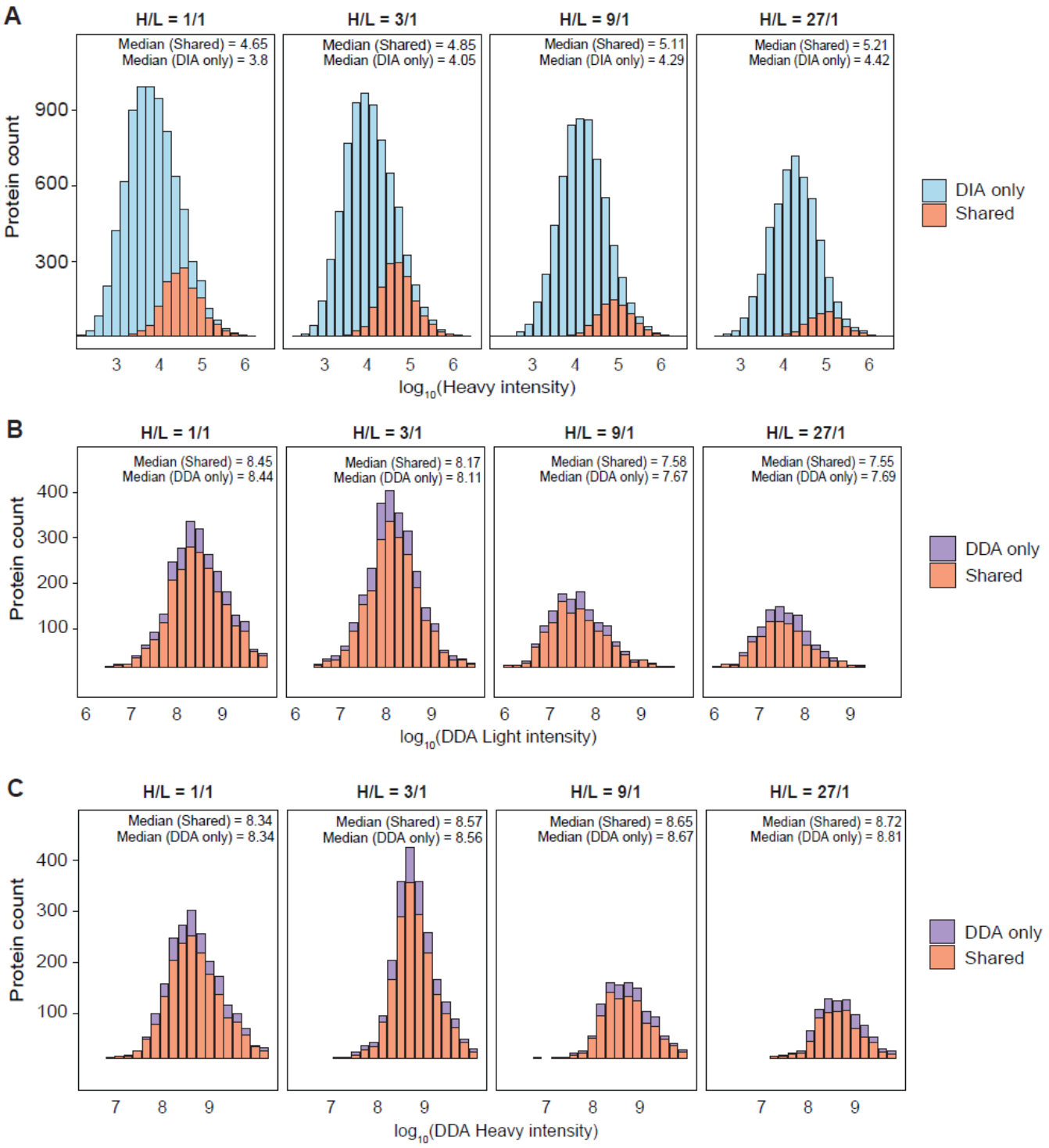

Figure S2. DIA improves proteome coverage by enabling quantitation of low-abundance precursors, related to Figure 1.

(A) Heavy peptide intensities for the DIA analysis of proteins quantified by both DIA and DDA compared to those quantified exclusively by DIA across standards with pre-defined H/L ratios. The median heavy intensities for two groups were labeled. Only proteins with CV < 20% for light, heavy intensities, H+L, and H/L ratios were included.

(B) Light peptide intensities for the DDA analysis of proteins quantified by both DIA and DDA compared to those quantified exclusively by DDA across standards with pre-defined H/L ratios. The median light intensities for

two groups were labeled. Only proteins with CV < 20% for light, heavy intensities, H+L, and H/L ratios were included.

(C) Same plots as in (B), using heavy intensities for the DDA analysis.

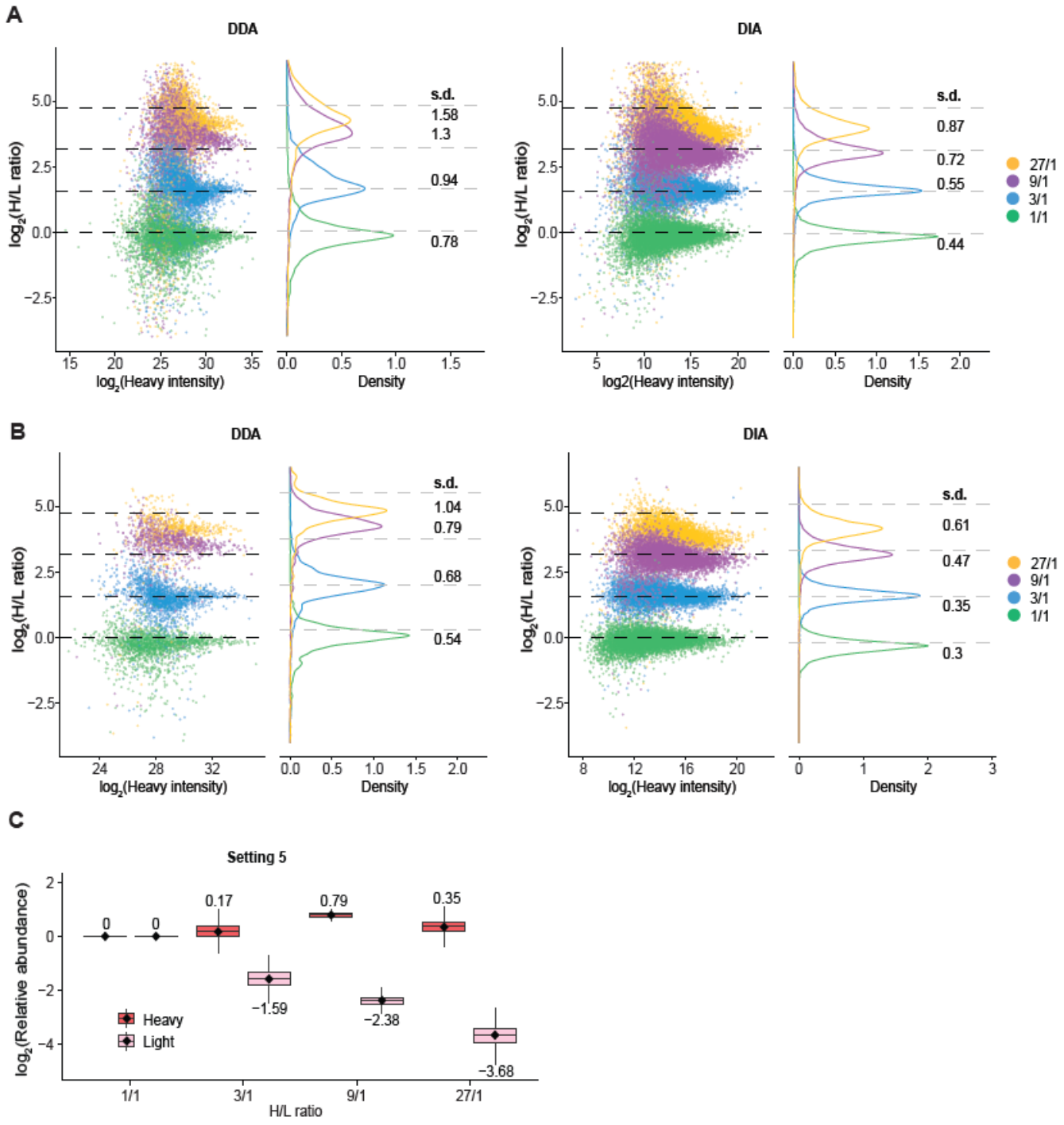

Figure S3. DIA enhances quantitation accuracy within and across samples, related to Figure 2.

(A) Scatter and density plots of heavy intensities for proteins quantified by DDA and DIA across different H/L ratios. s.d. indicates the standard deviation of $\log_2$(H/L) ratios within each group. Dashed lines mark the theoretical $\log_2$(H/L) values: $\log_2(1) = 0$, $\log_2(3) = 1.58$, $\log_2(9) = 3.17$, and $\log_2(27) = 4.75$.

(B) Same plot as in (A) but filtered using CV < 20% for light, heavy intensities, H+L, and H/L ratio; CVs were calculated when the protein is quantified in all three replicates.

(C) Quantification of light and heavy peptide intensities across standards with predefined H/L ratios based on DIA analysis using Setting 5 as described in Fig. S1A. Only proteins with CV < 20% for light, heavy intensities, H+L, and H/L ratios were included. Each dot and corresponding value represent the mean of measurements.

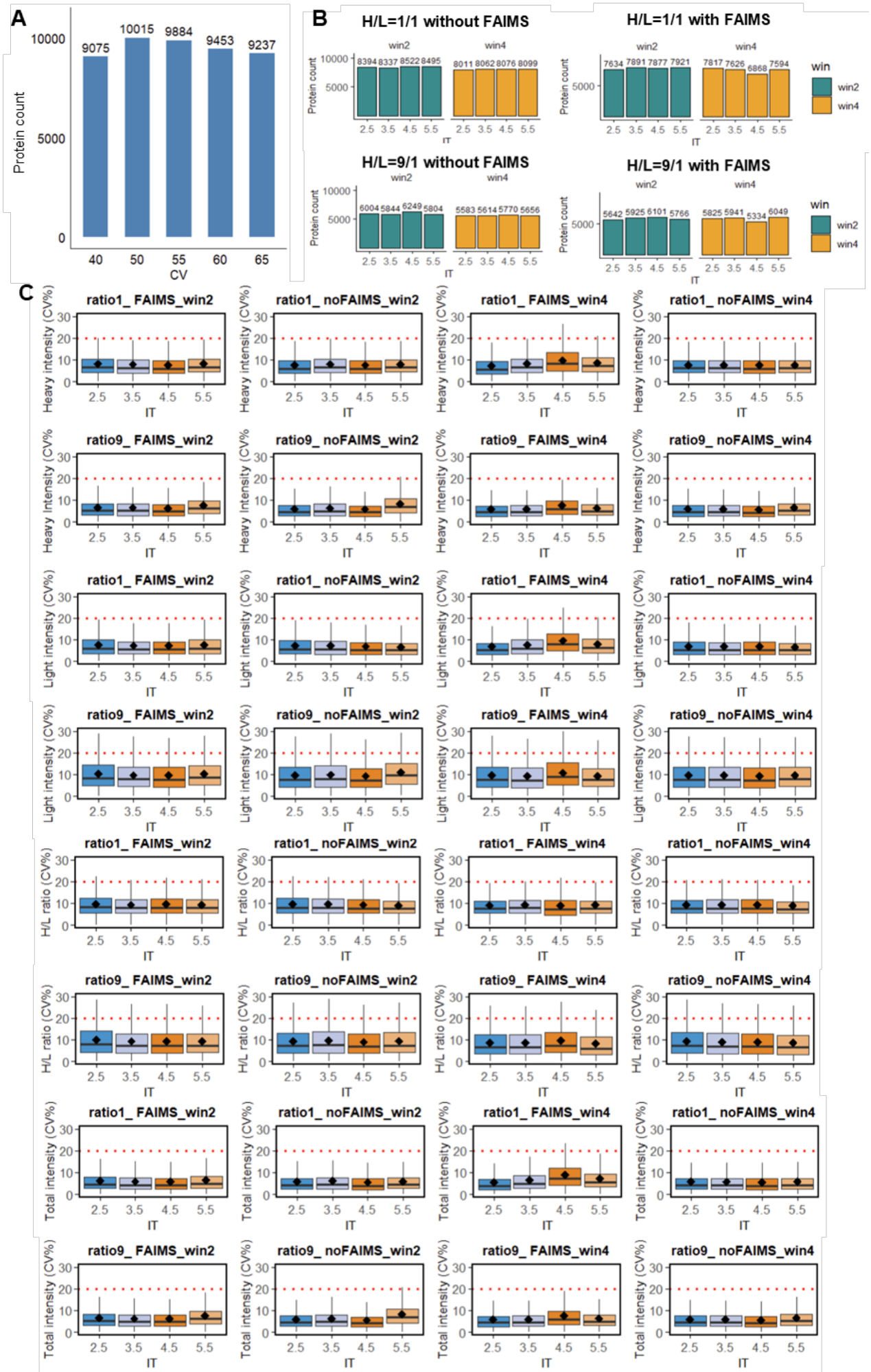
A
Protein count
CV
9075
10015
9884
9453
9237
B
H/L=1/1 without FAIMS
H/L=1/1 with FAIMS
H/L=9/1 without FAIMS
H/L=9/1 with FAIMS
win2
win4
Protein count
IT
win
C
ratio1_ FAIMS_win2
ratio1_ noFAIMS_win2
ratio1_ FAIMS_win4
ratio1_ noFAIMS_win4
ratio9_ FAIMS_win2
ratio9_ noFAIMS_win2
ratio9_ FAIMS_win4
ratio9_ noFAIMS_win4
Heavy intensity (CV%)
Light intensity (CV%)
H/L ratio (CV%)
Total intensity (CV%)
IT

Figure S4. DIA method optimization, related to Figure 1-2.

(A) Number of proteins quantified using FAIMS with different compensation voltages.

(B) Number of proteins quantified across different injection times (ITs), using 2 Th or 4 Th isolation windows, with or without FAIMS. Only proteins with CV < 20% for light, heavy intensity, H+L, and H/L ratios were included.

(C) CVs of heavy, light intensity, H+L, and H/L ratios under different instrument parameter settings.

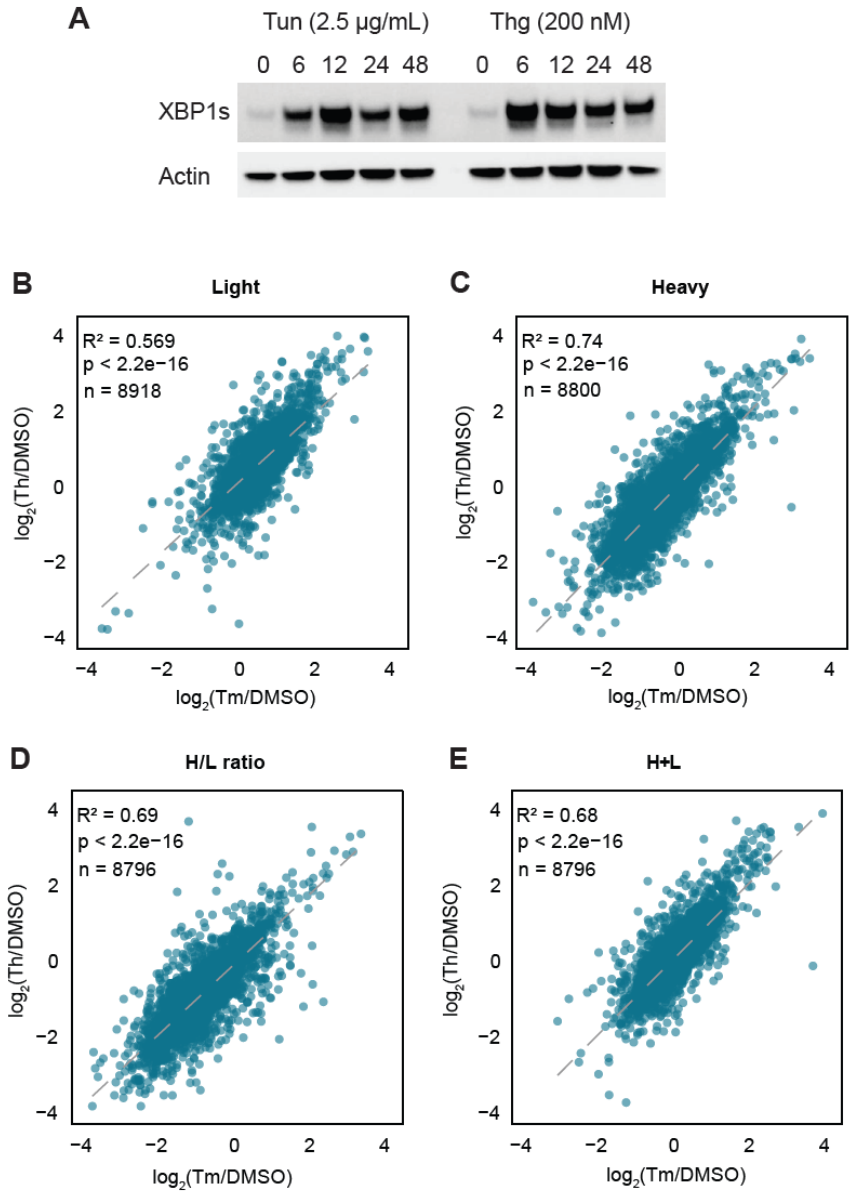

Figure S5. Th and Tm treatments resulted in correlated changes, related to Figure 3.

(A) Western blotting analysis of XBP1 protein levels in cells treated with 2.5μg/mL tunicamycin (Tm) or 200mM thapsigargin (Th) for 0, 6, 12, 24 and 48 hours.

(B) Correlation between $\log_2$(Th/DMSO) and $\log_2$(Tm/DMSO) for light intensities. n indicates the number of proteins included; R^2 is the Pearson correlation coefficient; p is the corresponding p-value.

(C) Same plot as (A), plotting using heavy intensities.

(D) Same plot as (A), plotting using H/L ratios.

(E) Same plot as (A), plotting using H+L.

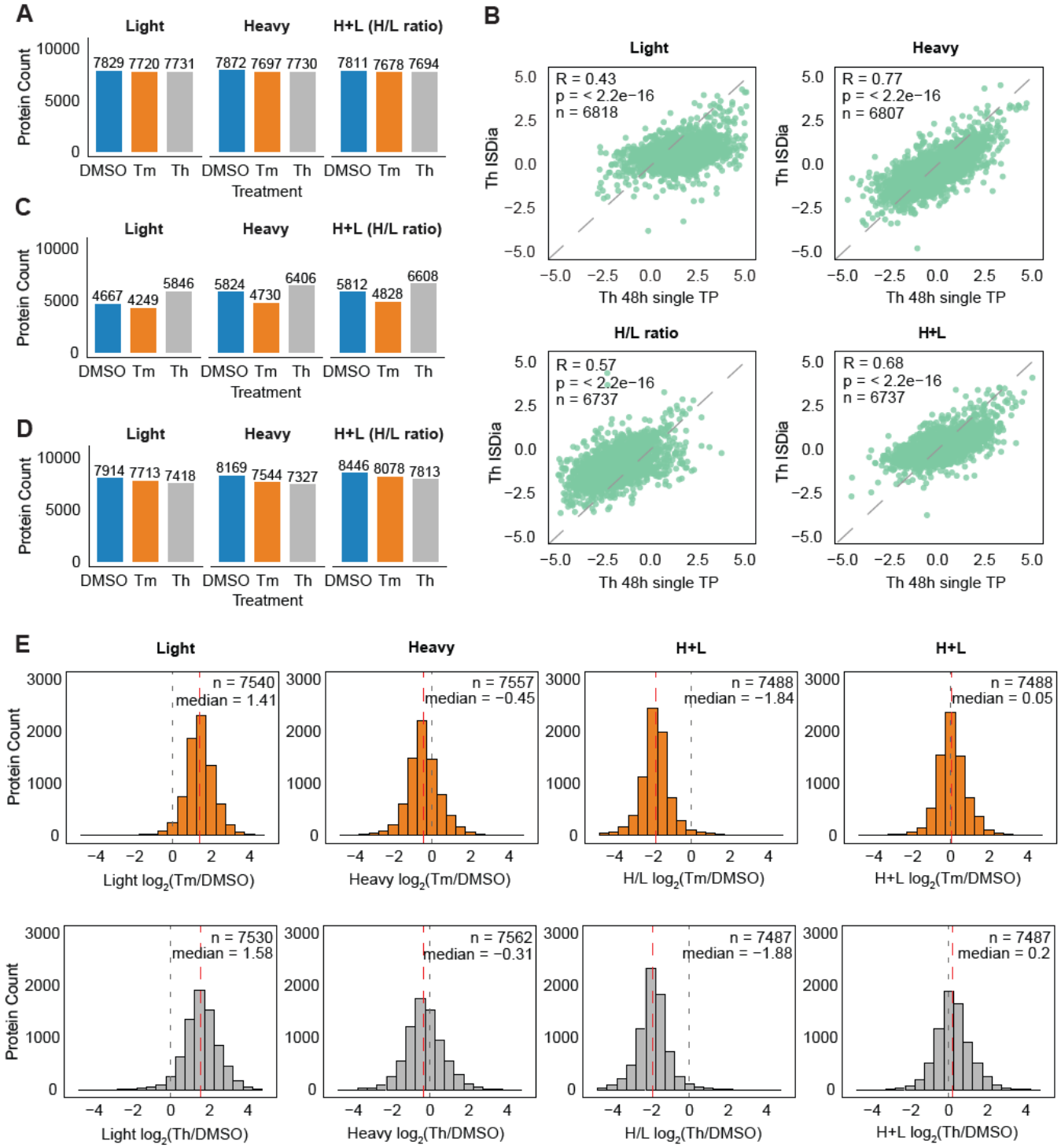

Figure S6. Comparison of ISDia and a single-timepoint ISDia approach, related to Figure 3.

(A) Number of proteins quantified with light, heavy intensity, and H+L (H/L ratio) across all three replicates at a

48-hour timepoint. H+L and H/L ratio values are included only when both light and heavy intensities were quantified.

(B) Pairwise comparison of log_2 fold changes in light, heavy intensity, H+L and H/L ratios derived from single-timepoint ISDia and ISDia intensities under Th and DMSO treatment conditions. n represents the number of proteins included; R is the Pearson correlation coefficient; p is the corresponding p-value.

(C) Number of proteins quantified with light, heavy intensity, H+L and H/L ratios in single-timepoint (48h) pSILAC-DIA. Proteins with CV < 20% for light, heavy intensity, H+L and H/L ratios were included, respectively.

(D) Same plot as in (C), showing data from ISDia.

(E) Distribution of log_2 fold changes for light, heavy intensity, H+L and H/L ratios across different treatment conditions relative to DMSO in single-timepoint (48h) ISDia. H+L and H/L ratio values were included only when both light and heavy measurements were available. n indicates the number of proteins included in each panel.

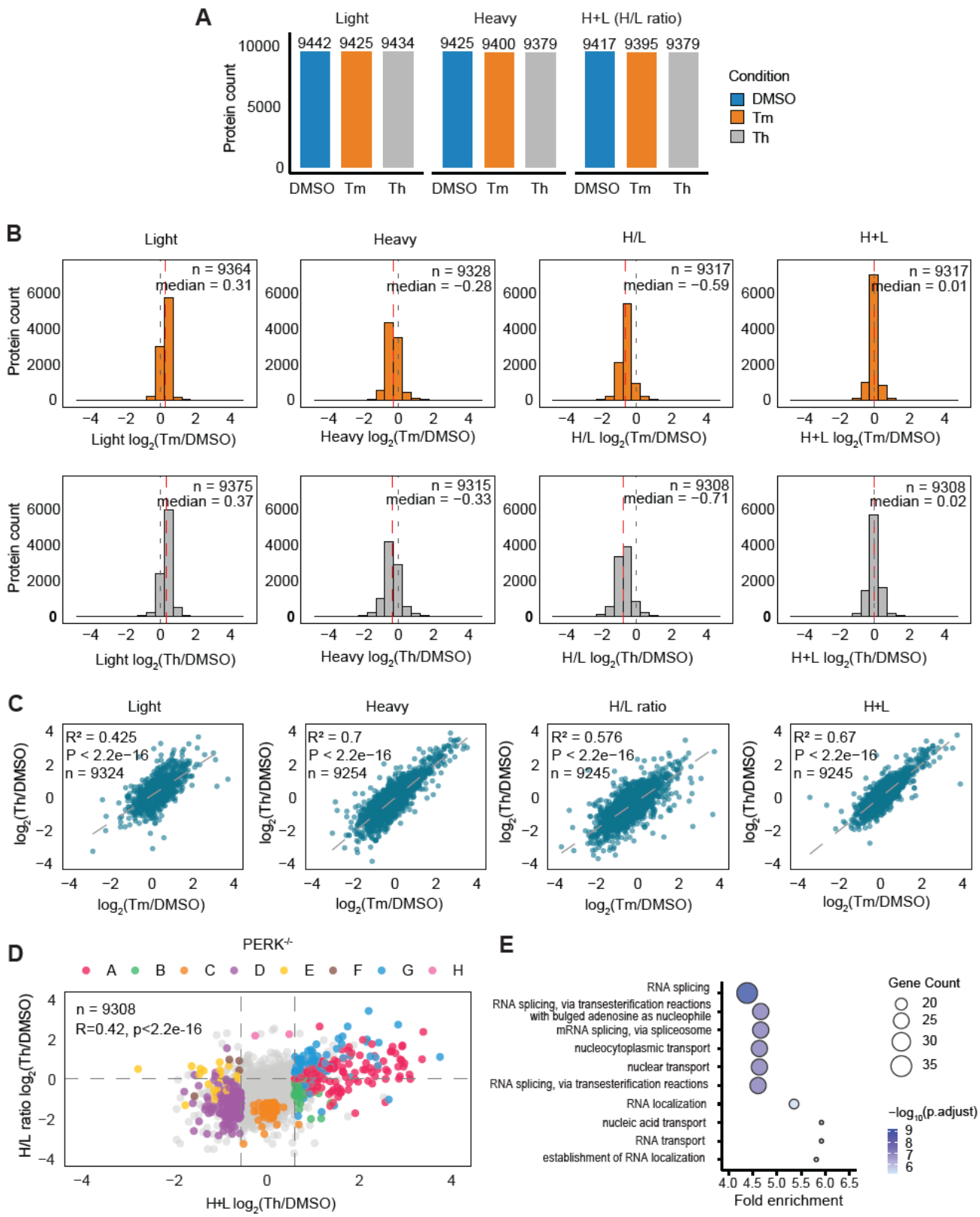

Figure S7. Protein dynamics in PERK$^{-/-}$ cells during the UPR using ISDia, related to Figure 4.

(A) Number of proteins quantified with light, heavy, and H+L (H/L ratio) across three replicates in each condition in PERK$^{-/-}$ cells. H+L and H/L ratio values are included only when the corresponding light and heavy intensities were quantified.

(B) Distribution of $\log_2$ fold changes for light, heavy intensity, H+L and H/L ratios in PERK^{-}/$^{-}$ cells under Tm (top)

and Th (bottom) treatments, relative to DMSO. H+L and H/L ratio were included only when both light and heavy intensity were quantified. n indicates the number of proteins included in each panel.

(C) Pairwise comparison of log_2(Th/DMSO) and log_2(Tm/DMSO) for light, heavy intensity, H+L and H/L ratios in PERK$^{-/-}$ cells. n indicates the number of proteins included in each panel; R^2 is the Pearson correlation coefficient; p is the corresponding p-value.

(D) Pairwise comparison of changes in H+L and H/L ratio under Th and DMSO treatment in PERK$^{-/-}$ cells. Each point represents a protein. The gray dashed lines indicate the fold change (FC) threshold of $log_2(1.5) \approx \pm 0.58$. Proteins are color-coded based on their changes across light, heavy, and H+L as follows: dark pink (up in light, heavy, and H+L); green (up in light and H+L, heavy not significant); orange (light up, heavy down, H+L l not significant); purple (down in heavy and H+L, light not significant); yellow (down in light, heavy, and H+L); brown (down in light and H+L, heavy not significant); blue (up in heavy and H+L, light not significant); light pink (light down, heavy up, H+L not significant); grey (others). Up is FC > 0.58 & p-value < 0.05; Down is FC < -0.58 & p-value < 0.05. n is the number of proteins shown; R is the Pearson correlation coefficient; p is the corresponding p-value.

(E) Biological processes enriched among proteins with significantly downregulated heavy and light intensity but H+L (Heavy log_2(Th/DMSO) < -0.58 & p-value < 0.05; Light log_2(Th/DMSO) < -0.58 & p-value < 0.05; H+L log_2(Th/DMSO): no significant change) in WT cells but heavy intensity were not significantly altered in PERK$^{-/-}$ cells under Th treatment compared to DMSO.

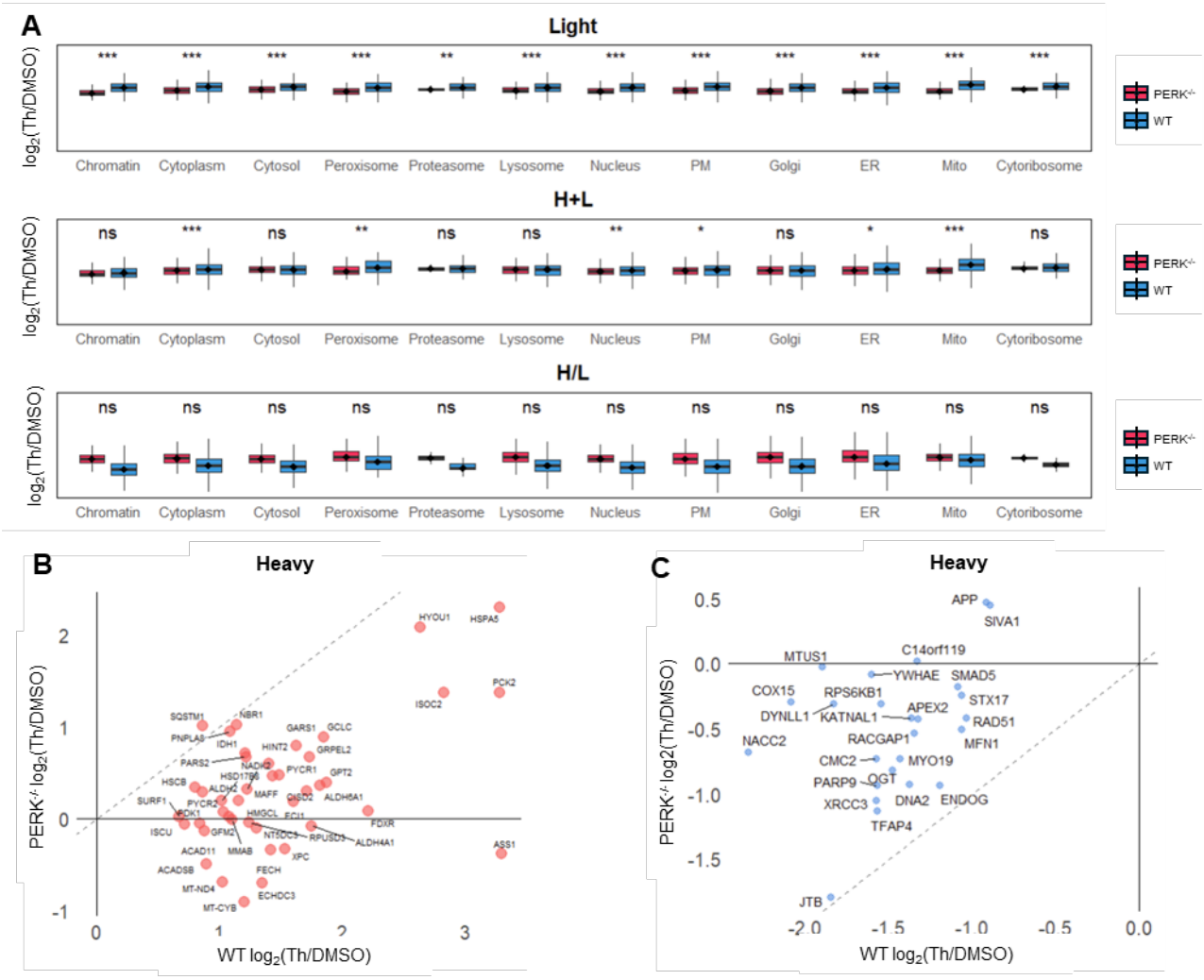

Figure S8. Protein dynamics analysis across cellular compartments during the UPR, related to Figure 5.

(A) Boxplot of $\log_2$(Th/DMSO) fold changes for light, H+L and the H/L ratio comparing WT and PERK$^{-/-}$ cells across subcellular compartments. P-values are from paired, one-tailed t-tests. *** $p < 0.001$; ** $0.001 < p < 0.01$; * $0.01 < p < 0.05$, ns, $p>0.05$.

(B) Scatter plot showing $\log_2$(Th/DMSO) changes in heavy peptide in WT and PERK$^{-/-}$ cells for mitochondrial proteins with potential increased synthesis and protein level in WT cells (Heavy $\log_2$(Th/DMSO) > 0.58 & p-value < 0.05; H+L $\log_2$(Th/DMSO) > 0.58 & p-value < 0.05; H/L $\log_2$(Th/DMSO) > 0).

(C) Same plot as in (B), showing the proteins with potential decreased synthesis and protein level in WT cells (Heavy $\log_2$(Th/DMSO) < -0.58 & p-value < 0.05; H+L $\log_2$(Th/DMSO) < -0.58 & p-value < 0.05; H/L $\log_2$(Th/DMSO) < 0), exclude Light $\log_2$(Th/DMSO) < -0.58 & p-value < 0.05).

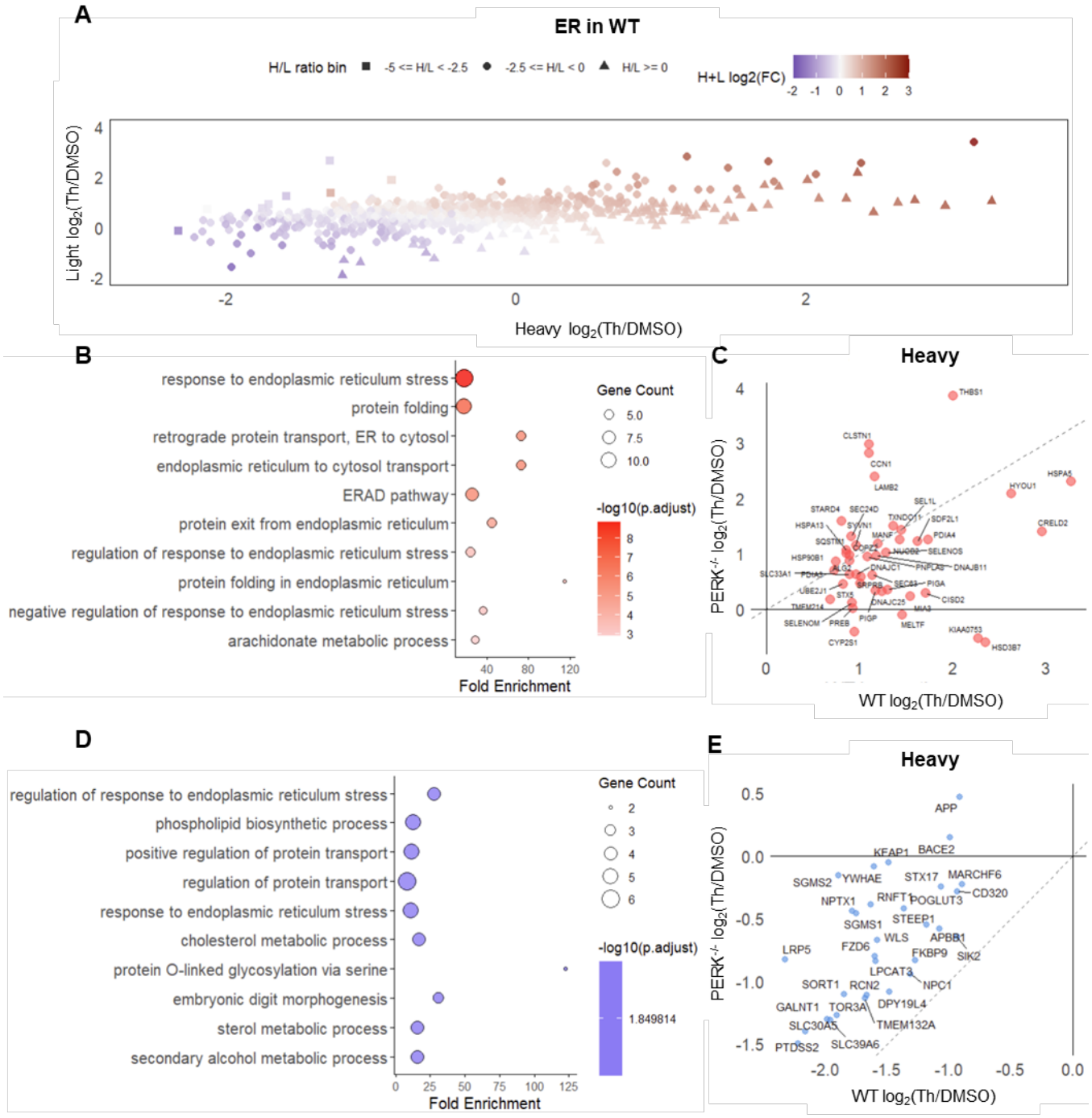

Figure S9. Analysis of protein dynamics in the ER, related to Figure 5.

(A) Bubble plots showing $\log_2$(Th/DMSO) changes in light, heavy intensity, H+L and H/L ratios in ER in WT cells.

(B) Biological processes enriched among the ER proteins with potential increased protein synthesis (Heavy $\log_2$(Th/DMSO) > 0.58 & p-value < 0.05; H+L $\log_2$(Th/DMSO) > 0.58 & p-value < 0.05; H/L $\log_2$(Th/DMSO) > 0) in WT cells.

(C) Scatter plot showing $\log_2$(Th/DMSO) changes in heavy peptide intensity in WT and PERK$^{-/-}$ cells for ER proteins in (B).

(D) Biological processes enriched among the ER proteins with potential decreased protein synthesis (Heavy $\log_2$(Th/DMSO) < -0.58 & p-value < 0.05; H+L $\log_2$(Th/DMSO) < -0.58 & p-value < 0.05; H/L $\log_2$(Th/DMSO)

< 0 but not Light $\log_2$(Th/DMSO) < -0.58 & p-value < 0.05) in WT cells.

(E) Same plot as in (C), showing the proteins in (D).

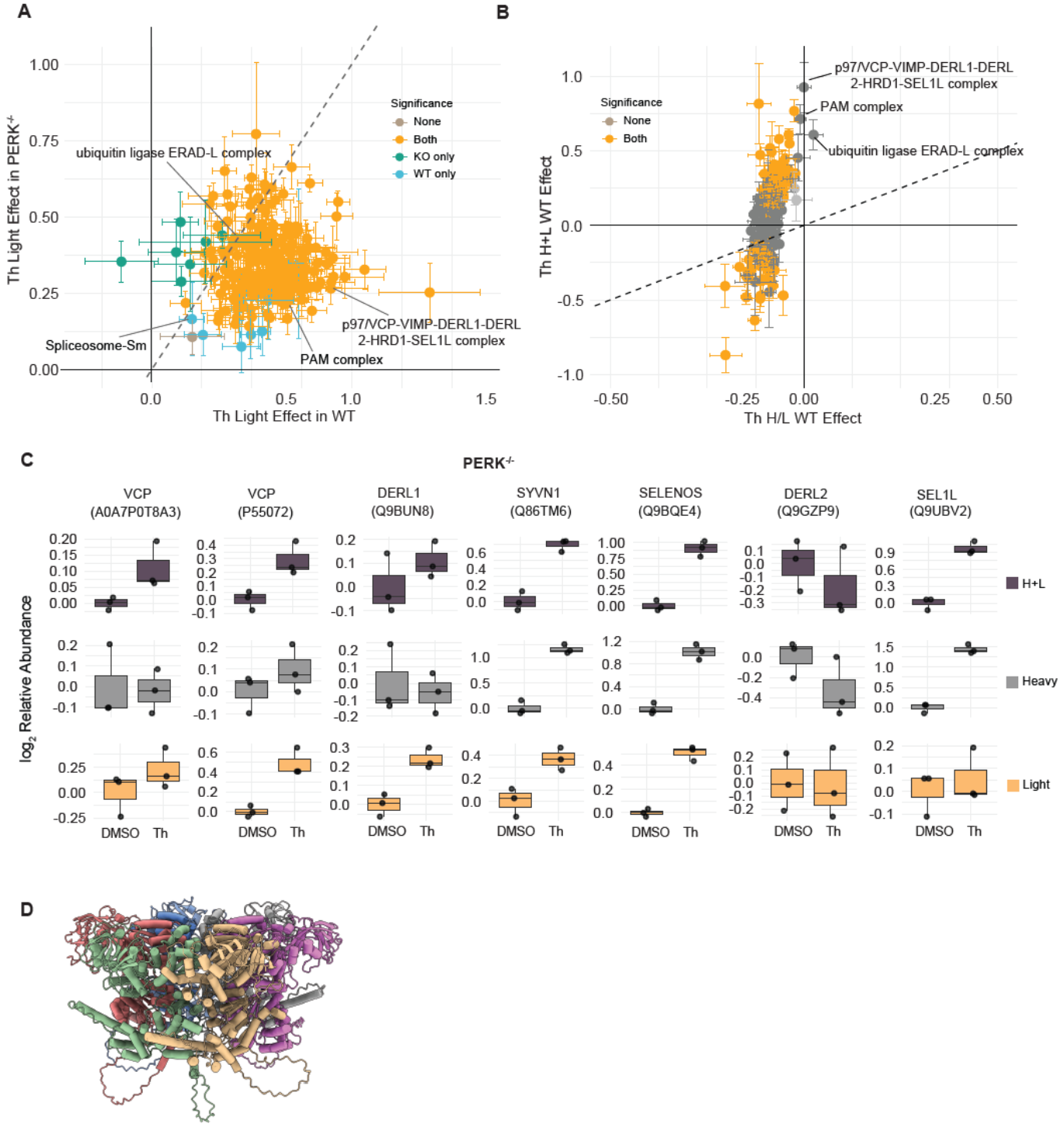

Figure S10. Dynamic regulation of protein complexes under UPR stress, related to Figure 6.

(A) Pairwise comparison of H+L and H/L ratios of protein complexes in WT cells under Th treatment relative to DMSO. Significance was indicated based on p-value < 0.05.

(B) Pairwise comparison of effects on light intensities on protein complexes under Th treatment relative to DMSO in WT and PERK$^{-/-}$ cells.

(C) Boxplot of the relative changes of H+L, heavy and light intensities under Th treatment relative to DMSO for subunits of the p97/VCP-VIMP-DERL1-DERL2-HRD1-SEL1L complex in PERK$^{-/-}$ cells.

(D) Side view of the AlphaFold3-predicted hexameric structure of the short P97/VCP isoform (UniProt ID: A0AP0T8A3), with each protomer uniquely colored for clarity.

Supplemental Table Legend

Table S1. Changes in heavy and light peptide intensities, as well as H+L and H/L ratios, under Th or Tm treatment in WT cells. Cellular compartments are annotated. Related to **Figure 3**.

Table S2. Changes in heavy and light peptide intensities, as well as H+L and H/L ratios, under Th or Tm treatment in PERK$^{-/-}$ cells. Cellular compartments are annotated. Related to **Figure 4**.

Table S3. Changes in heavy and light peptide intensities, as well as H+L and H/L ratios of protein complexes, under Th or Tm treatment in WT and PERK$^{-/-}$ cells. Related to **Figure 6**.